DEVELOPING NEW CLASSES OF ACOUSTOFLUIDIC SYSTEMS

A Dissertation

by

SINAN YIGIT

Submitted to the Office of Graduate and Professional Studies of
Texas A&M University
in partial fulfillment of the requirements for the degree of

DOCTOR OF PHILOSOPHY

Chair of Committee,	Arum Han
Committee Members,	Raffaella Righetti
	Victor Ugaz
	Jun Zou
Head of Department,	Miroslav M. Begovic

December 2019

Major Subject: Electrical Engineering

ABSTRACT

As being one of the contactless and label free methods in microfluidics, acoustofluidics has provided great benefits to the researchers in terms of cell/particle analysis, separation, and screening. This recent technology uses the particle handling phenomenon of acoustics wave in microfluidic platforms and lets scientists benefit contact-free and effective particle and cell manipulation in the field of microfluidics. Throughout this study, four different acoustofluidic platforms have been designed, fabricated and tested to promote the abundant usage of acoustofluidics technology.

The first and second chips were designed to enable cell/particle position change in an acoustic microfluidic chip since position of particles/cells inside the acoustofluidic chip is strictly dependent on the channel geometry and it is fixed once the microfluidic platform is fabricated. To solve this restriction, fluidic boundary needs to be separated from the acoustic boundary. In the first study, acoustofluidic platform with two adjacent microchannels were designed. One of the microchannels was used to flow particles/cells, and second microchannel with staircase structure was used to change the position of particles/cells inside the main microfluidic channel by changing the effective channel width. Using this chip we successfully demonstrated the particle position change inside the main microfluidic channel. The second acoustofluidic platform was designed and fabricated by filling the side of microfluidic channel with a transparent material, polydimethylsiloxane (PDMS) so that position of acoustic pressure nodes can be adjusted depending on the width of the PDMS slab. By the help of soft-lithography techniques

PDMS wall could be successfully integrated into side of the microfluidic channel in a cost-effective manner since previous studies required expensive equipment such as laser to integrate the PDMS slab. Fabrication of this acoustofluidic chip was implemented and yielded successful results of particle manipulation by the help of acoustophoresis when tried with different types of particles. In the third acoustofluidic chip flow control capability for on-chip laboratory studies was enabled since acoustofluidic platforms lack on-chip flow control attribute. For that reason, microvalves were designed and integrated into acoustofluidic platform so that scholars who study particle/cell manipulation requiring on-chip flow control can benefit and modify this method. This platform was also successfully fabricated and used for on-chip culture medium exchange to enable intra-droplet cell culture. The last platform was to integrate acoustofluidic technology with droplet microfluidics so that acoustic platforms can take advantage of droplet microfluidics since they provide efficient cell screening, high throughput, and ability to run parallel experiments. Outcome of fabricating this chip was also rewarding and preliminary experiments to test this platform showed promising results for future works.

To summarize, since acoustofluidics is an emerging and rapidly growing technology and science field in last two decades some of the limitations arose in this technology. Those restrictions are addressed in the following sections and alternative fabrication methods to solve those restrictions and the outcome of those methods are discussed.

To my wife, my daughter and my parents
for their endless love, support, patience and encouragement

ACKNOWLEDGEMENTS

I would like to express my sincerest gratitude to my research advisor, Dr. Arum Han. This dissertation would have been impossible without his ongoing support, guidance, insight, and encouragement, which not only helped me to finish the doctoral study but also will make me gain necessary skills for my professional development. I also would like to thank my committee members, Dr. Jun Zou, Dr. Rafaella Righetti, and Dr. Victor Ugaz for their advice and support.

I gratefully acknowledge the Ministry of National Education of the Republic of Turkey and people of Turkey for their financial support during my study. Without this financial support, finishing my studies would be a real challenge for me.

I would like to acknowledge all group members in the NanoBio Systems lab for their friendship, help and understanding. I especially thank Dr. Younghak Cho and Dr. Han Wang for their generous help and guidance throughout my research.

I am thankful to have wonderful friends: Dr. Celal Erbay, Dr. Ali Riza Ekti, and any others I did not list. Thank you for all your warm friendship and support.

Last but not least, I would like to thank to my family. Without their love and support it would not be easy for me to succeed.

CONTRIBUTORS AND FUNDING RESOURCES

Contributors

This dissertation was supervised by Prof. Arum Han. Silicon microchannels of the acoustofluidic platforms were fabricated by Nano-bio Systems Laboratory (Prof. Younghak Cho) in Seoul National University of Technology, Korea.

All other work conducted for this dissertation was completed by the student independently.

Funding Sources

Graduate student was supported by a fellowship from the Ministry of National Education of the Republic of Turkey.

TABLE OF CONTENTS

Page

LIST OF FIGURES

Page

LIST OF TABLES

Page

1. INTRODUCTION

1.1. Theory of Acoustophoresis

An acoustic wave can be defined as longitudinal and mechanical wave resulting from an oscillation of pressure where at longitudinal wave propagation direction is same with vibration direction. Similar to the other waves wavelength of an acoustic wave is the distance between the two equilibrium points and shown as:

$$\lambda = \frac{v}{f} \tag{1}$$

Where 'v' represents the speed of sound inside the medium sound propagates and 'f' is the frequency of the sound wave.

An acoustic wave can be shown as a function of time:

$$f(t) = A\sin(\omega t + \phi) \tag{2}$$

Where `$A$` denotes the peak value of the function, `$\omega$` is $2\pi f$ as angular frequency and `$\Phi$` is the phase shift of the acoustic wave. King [1], Yosioka and Kawasima [2] have studied the theory of acoustic wave forces on spherical objects. The force exerted on a spherical particle is called acoustophoretic force and can be shown as:

$$F_a = -\left(\frac{\pi p^2 V_0 \beta_s}{2\lambda}\right)\phi(\beta,\rho)\,sin(2ky) \tag{3}$$

Where `$p$` is defined as the acoustic pressure amplitude, and `$V_0$` is volume of the particle, `$\beta_s$` is compressibility of the medium surrounding the particle, `$\lambda$` is wavelength of the

acoustic wave, `$k$` is the wavenumber, and `$\Phi$` is the acoustic contrast factor. And acoustic contrast factor is expressed as:

$$\phi(\beta,\rho) = \frac{5\rho_0 - 2\rho_s}{2\rho_0 + \rho_s} - \frac{\beta_0}{\beta_s} \tag{4}$$

Where `$\beta_0$` is compressibility of the particle, and `$\rho_0$` is the density of the particle, `$\rho_s$` is the density of the medium. Depending on acoustic contrast factor being positive or negative, the position where particles migrate changes. If it is positive the particles move to the position where the amplitude of the acoustic wave motion is thought to be zero. Otherwise they migrate to the locations where the amplitude of motion is high. The position where motion is zero is called acoustic pressure node and the nodes where acoustic wave motion is thought to be maximum is are called acoustic pressure anti-nodes. This phenomenon was illustrated in **Fig. 1.1** by defining the half sinusoidal wavelength between two solid walls.

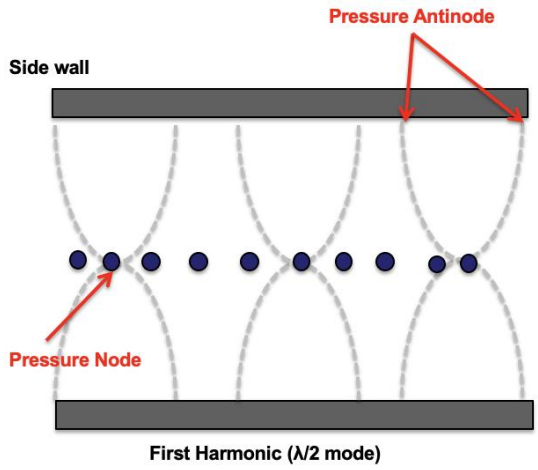

Figure 1.1 Illustration of particle migration to acoustic pressure nodes

1.2. Principles of Acoustofluidics

As a science and technology microfluidics deals with the fabrication of channels with dimensions in micrometer-scale, and also interested in flow and manipulation of liquids and suspended particles/cells in small amount of liquids in those fabricated channels [3, 4]. Fabricating the channels in micro scale let scientists take advantage of neglecting the physical forces in macro-scale [5]. The advantages for using microfluidic devices are easy, low-cost fabrication, high-throughput capabilities, low consumption of media, cells, and flexibility based on the analyzed particle/cell size. Integration of external fields such as dielectric field, magnetic field, and acoustic field let researchers manipulate particle/cells precisely. The integration of those fields is very useful for different type of applications like particle/cell property analysis, sorting, and enrichment. To mention some of them: dielectrophoresis [6, 7], magnetophoresis [8, 9], hydrodynamic separation [10, 11], and acoustophoresis [12].

As being one of the methods used in microfluidics, acoustofluidics deals with the application of acoustic waves in microfluidic environments so that migration with sound so called acoustophoresis is implemented [13]. Acoustophoresis is a contactless and label-free method to manipulate particles/cells based on their physical properties like size, shape, density, and compressibility [14]. Some of the applications using acoustofluidics in the literature are positioning and trapping of cells [15, 16, 17, 18], streamline focusing of particles [19, 20], cell-property analysis using flow cytometry [21, 22], particle property analysis [23, 24]. Besides that, acoustophoresis method was combined with other microfluidics techniques. To name a few: dielectrophoresis [25, 26], droplet microfluidics

[27, 28, 29, 30]. Another application to employ acoustofluidics is used for isolating exosomes from cells [31]. It is important to note that in this study Wu et. al. achieved a throughput of 4 microliter per hour (μL/h) and the separation efficiency of the microfluidic chip was ~98% as being a good example of high throughput and efficiency of acoustofluidic platforms.

To date a variety of particle and cell manipulation applications have been developed using bulk acoustic wave (BAW)-based acoustofluidic systems. The principle of those systems lies on the phenomena that particles passing through acoustic resonance field, namely acoustic standing wave created between the two side channels of a microfluidic channel functioning as half-wavelength resonators, move towards positions in the microfluidic channel called acoustic pressure nodes and/or anti-nodes depending on their acoustic contrast factor. Depending on the frequency applied through the piezoelectric transducer generating the acoustic wave, these acoustic pressure nodes are generated in the ½ position, ¼ and ¾ positions, and so on of the microfluidic channel width. The major benefits of bulk acoustofluidic technology is that it can provide contactless and label-free manipulation of particles, including cells, in microscale applications with extremely simple microstructures and instrument setup.

Acoustofluidic devices are generally called as acoustic resonators. The first type of acoustic resonator is surface acoustic wave (SAW) resonator. In this resonator-type, electrodes (interdigitated transducers-IDTs) are fabricated on the piezoceramic substrate such as lithium niobite ($LiNbO_3$) [32] and the channel structure is made of materials which have similar acoustic impedance with water such as PDMS. The reason for choosing low

acoustic impedance material is to minimize the loss based on channel geometry. As illustrated in **Fig. 1.2** SAW resonators consist of at least two IDTs on each side and a channel structure between those transducers. The acoustic wave is generated by those IDTs and depending on the wavelength of the acoustic wave and the size of the particles/cells they are manipulated to certain positions inside microfluidic channel.

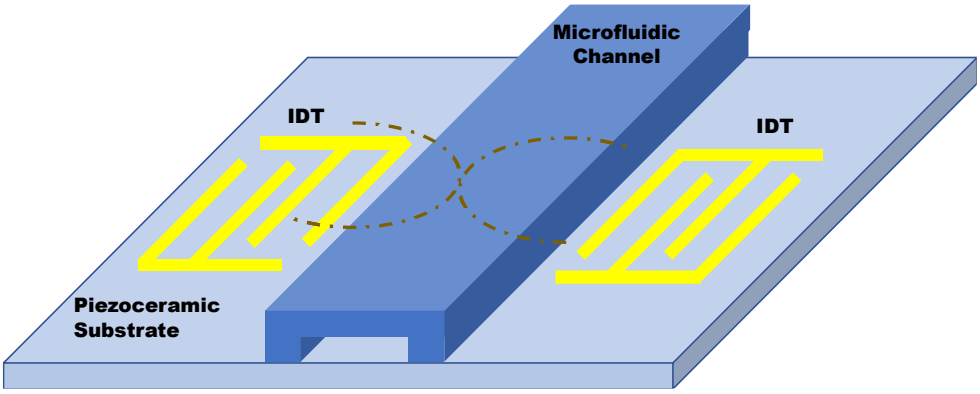

Figure 1.2 Illustration of Surface Acoustic Wave Resonator (Redrawn from Ref [33])

As being one of the other two acoustic resonator types, layered acoustic resonators as shown in **Fig. 1.2**, are usually configured as a resonance channel with geometrically designed layers, such as reflector layer, fluid layer, transmission layer and coupling layer and they are referred as planar resonators. Each layer thickness needs to be accordingly designed so that wave can travel with little or no loss. The transducer at the bottom generates the acoustic wave by vibrating at certain frequency and voltage. Coupling layer plays a role to transmit the wave from the transducer to the chip. The bottom of the resonator channel is formed by the matching serving also as the acoustic wave reflector.

The medium layer carries the particles or cells which are suspended in the liquid. The top of the resonator chip is formed by the reflector layer and its role to reflect the acoustic wave. In some cases, second transducer can be employed instead of reflector layer so that acoustic wave can be generated at the same frequency from both sides. Therefore, resonance will occur inside the channel. Using this method will let researcher change the particle/cell position inside the channel. The matching layer and reflector need to have quarter wavelength thickness as shown in **Fig.1.3A** and the fluid layer should be kept at half wavelength thickness to minimize the acoustic attenuation [34]. And the whole body should operate near fundamental resonance frequency of the transducer.

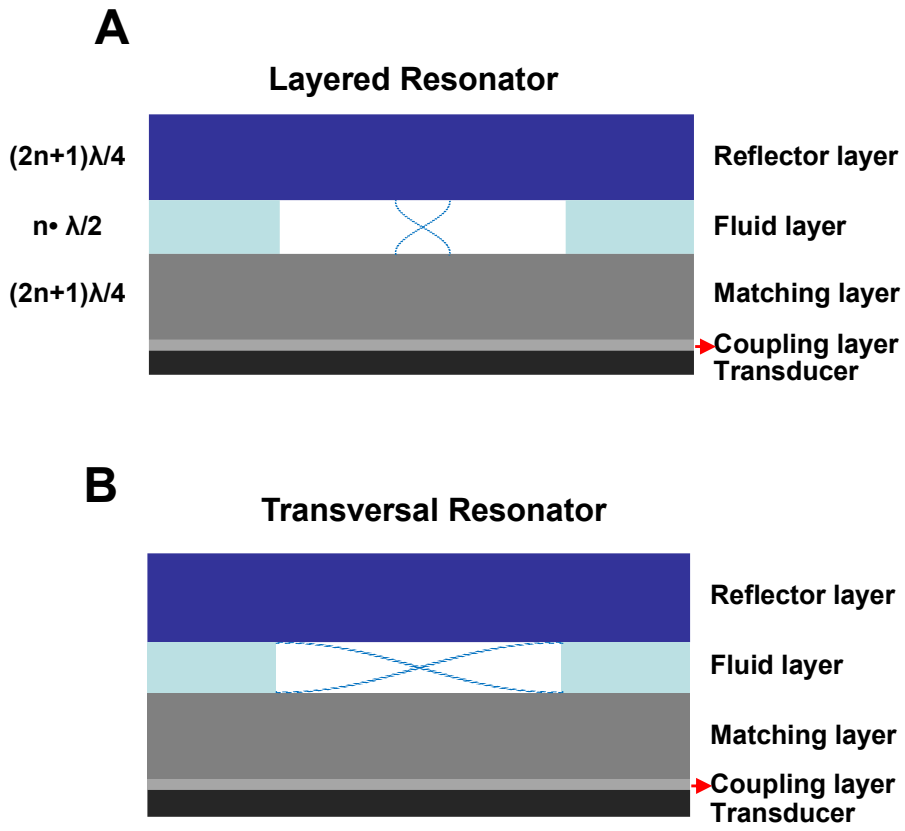

Figure 1.3 Illustrations of the different configurations of acoustic resonators: **(A)** Layered resonator, **(B)** Transversal resonator (Redrawn from Ref [33])

Second configuration type for acoustic resonators is transversal resonator. In this configuration the acoustic wave is formed perpendicular to the generation direction of the transducer. Using this method will let the acoustic wave be reflected between the sidewalls of the fluidic channel. This is realized by vibrating the whole chip as one body. Because of that material selection is limited to avoid the acoustic attenuation loss. In these resonator systems materials with high acoustic impedance, Z, such as glass, silicon, polymethyl-methacrylate (PMMA), and metals are preferred so that loss can be minimized. As

illustrated in **Fig.1.3B** these resonator systems are not affected by the thickness of each layer.

As mentioned above, acoustic impedance of the material is denoted by Z and calculated by multiplying the density of the material by transversal speed of sound in that material:

$$Z = \rho c \tag{5}$$

Table 1.1 provides the acoustic impedance of most commonly used materials in acoustofluidics. It is important to note that while planar resonators may use low acoustic impedance materials such as polydimethylsiloxane (PDMS), the transversal resonator requires usage of high acoustic impedance materials such as silicon and glass.

Table 1.1 Density, speed of sound and characteristic acoustic impedance of most commonly used materials in acoustofluidics (Reprinted from [33])

Materials	***Density ($kg \bullet m^{-3}$)***	***Speed of sound ($m \bullet s^{-1}$)***	***Acoustic Impedance ($10^6\ kg \bullet m^{-2} \bullet s$)***
PZT (Piezoceramic)	7700	4000	30.8
Silicon	2331	8490	19.79
Borosilicate Glass	2230	5647	12.59
Steel-stainless 347	7890	5790	45.68
Polymethacrylate	1150	2590	2.98
Polydimethylsiloxane	965	1119 (5:1)	1.08
H_2O(25°C)	997	1497	1.49

Though PDMS is also used as a structural material in this work to fabricate acoustic microfluidic platform silicon and borosilicate glass was the main substrates while fabricating acoustofluidic chips because of their high acoustic impedance.

Here it is worth note that acoustofluidics can employ high throughput separation in microfluidics without sacrificing the separation efficiency unless other microfluidic techniques. The following table summarizes the separation efficiency and throughput values of conventional methods in microfluidics. As shown in **Table 1.2** comparison of efficiency and throughput of microfluidic methods. Even though acoustofluidics has the second highest throughput it is more advantageous than immunoaffinity methods since this method makes contactless and label-free separation possible without necessity of antibody efficacy studies. Also, it must be pointed out that in this comparison acoustofluidics use the SAW based acoustic microfluidic platform for whole-blood separation into exosomes, red blood cells, and white blood cells.

Table 1.2 Comparison of different exosome separation methods in microfluidics and their separation performance (Reprinted from [35])

Microfluidic Methods	***Isolation principle***	***Yield (%)***	***Purity (%)***	***Throughput***
Microfluidic immunoaffinity (ExoChip) [36]	Antibody capture	42–94	87–97	8–16 μl/min
Dielectrophoretic (DEP) Separation [37]	Size, polarizability, and dielectrophoretic force	Not described	Not described	~30 min
Ciliated micropillars Isolation [38]	Size difference	15–60	Not described	~10 min
Deterministic lateral displacement (DLD) [39]	Size difference	Not described	Not described	0.1–0.2 nL/min
Acoustofluidics [31]	Size and acoustic contrast factor	~82	~98	4 μL/min

1.3. Objective of the Work and Chapter Outlines

It is undeniable that microfluidic platforms are exploited extensively in life science research and medicine because of their portability, requiring small volume of sample and allowing rapid diagnostics [40]. As being one of the popular methods in microfluidics acoustofluidics has been worked extensively because of its high-throughput and label-free manipulation. Being used intensively let researchers report some limitations of those platforms depending on geometrical parameters, material selection, etc. Dependency and uncertainty of geometrical and material parameters in these platforms made experimental

characterization inevitable so that their successful application to manipulate cells or particles can be characterized [41].

The aim of this study to eliminate some of the limitations in acoustofluidic platforms suffer by using either new fabrication techniques or integrating conventional microfluidic methods into acoustofluidic platforms and characterize successful operation of those platforms by running experiments. The next chapter mentions about a very common limitation which acoustofluidic devices suffer. since acoustic pressure nodal planes are fixed in an acoustic microfluidic chip geometry dependence of acoustofluidic platforms limits its plentiful usage. In that manner, acoustofluidic platform was designed to have different acoustic pressure nodal planes so that the particles can be dragged into different nodal planes. In that chapter, design considerations for acoustofluidic platforms with different channel dimensions are mentioned and experimental results of successfully fabricated acoustofluidic device with varying pressure nodal positions are summarized.

The third chapter provides an alternative method to solve the limitation mentioned in the second chapter. In this method acoustic boundary is decoupled from the fluidic boundary by implementing appropriate fabrication methods. For that purpose, simulation using the finite element analysis method was run to assess preliminary data of acoustic pressure nodal planes after PDMS wall integration. Following the simulation, a novel method to integrate PDMS wall into acoustofluidic platform using soft lithography was summarized and the successfully fabricated acoustofluidic chip was tested using positive acoustic contrast and negative acoustic contrast particles.

In the fourth chapter another attribute which acoustofluidic platforms require was discussed. Bulk acoustic wave (BAW) based acoustofluidic platforms lack of on-chip flow control since they are made of high acoustic impedance materials such as silicon and glass. To provide on-chip fluid flow control microvalves were integrated into the acoustofluidic platform. Fabrication steps to integrate microvalve structure were summarized and experimental characterization of this platform was successfully implemented by trapping hydrogel droplets inside an acoustofluidic platform and changing the surrounding medium by operating the microvalves.

Fifth chapter mentioned the design consideration of an acoustofludic platform which is capable of particle manipulation inside droplets. To generate droplets, T-junction droplet generator was integrated into an acoustofluidic platform so that acoustofluidic chip could take some advantages of droplet microfluidics such as high throughput, being scalable, and being capable of running simultaneous experiments [42]. In that acoustofluidic platform positive acoustic contrast particles were encapsulated by an aqueous phase droplet and oil was used as spacer between each droplet. Acoustofluidic device with droplet generator was successfully fabricated and functionality was confirmed at different acoustic wave modes.

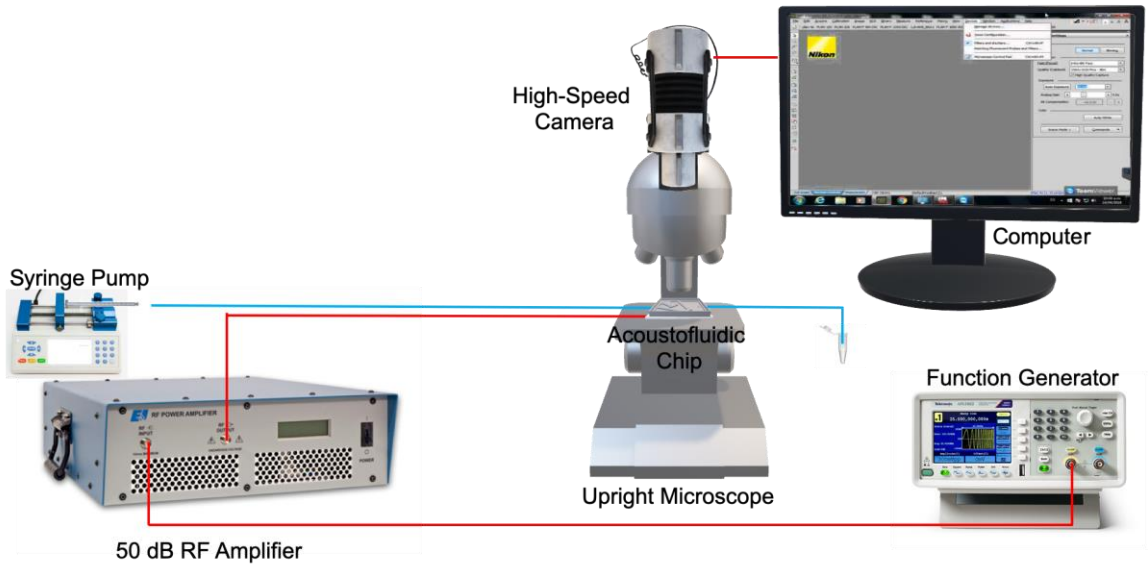

Figure 1.4 Experimental setup to run the acoustofluidic experiments

The experimental setup to test the fabricated acoustofluidic platforms was illustrated in **Fig. 1.4**. The setup consists of imaging, flowing, acoustic generation, analysis equipment. For imaging purposes upright fluorescence microscope (Nikon Inc, NY, USA) and high-speed camera (Hamamatsu Orca-Flash4.0, Japan) were operated. To flow particles/cells syringe pumps (Chemyx Fusion 200/400, TX, USA) were run to push the fluid inside the syringes and once the fluid with cells/particles passes through the microfluidic platform it was collected in a small vial or tube. Microscopic images were analyzed on a desktop computer which NIS software was installed into. To generate the acoustic waves function generator (Tektronix AFG3021B, OR, USA or Rigol DG4202, OR, USA) was connected to a power amplifier (ENI 2100L Linear Power Amplifier, Bell Electronics, WA, USA) so that PZT can be actuated.

References

1. King LV. On the acoustic radiation pressure on spheres. Proceedings of the Royal Society of London. Series A-Mathematical and Physical Sciences. 1934 Nov 15;147(861):212-40.
2. Hasegawa T, Yosioka K. Acoustic- radiation force on a solid elastic sphere. The Journal of the Acoustical Society of America. 1969 Nov;46(5B):1139-43.
3. Terry SC, Jerman JH, Angell JB. A gas chromatographic air analyzer fabricated on a silicon wafer. IEEE transactions on electron devices. 1979 Dec;26(12):1880-6.
4. Manz A, Harrison DJ, Verpoorte EM, Fettinger JC, Paulus A, Lüdi H, Widmer HM. Planar chips technology for miniaturization and integration of separation techniques into monitoring systems: capillary electrophoresis on a chip. Journal of Chromatography A. 1992 Feb 28;593(1-2):253-8.
5. Bruus H. Theoretical microfluidics. Oxford: Oxford university press; 2008 Jan.
6. Gascoyne PR, Vykoukal J. Particle separation by dielectrophoresis. Electrophoresis. 2002 Jul;23(13):1973-83.
7. Neumann E, Sowers AE, Jordan CA. Plenum Press; New York: 1989. Electroporation and Electrofusion in Cell Biology.
8. Zborowski M, Ostera GR, Moore LR, Milliron S, Chalmers JJ, Schechter AN. Red blood cell magnetophoresis. Biophysical journal. 2003 Apr 1;84(4):2638-45.
9. Pamme N, Wilhelm C. Continuous sorting of magnetic cells via on-chip free-flow magnetophoresis. Lab on a Chip. 2006;6(8):974-80.

10. Lieu VH, House TA, Schwartz DT. Hydrodynamic tweezers: Impact of design geometry on flow and microparticle trapping. Analytical chemistry. 2012 Feb 3;84(4):1963-8.
11. Yamada M, Seki M. Hydrodynamic filtration for on-chip particle concentration and classification utilizing microfluidics. Lab on a Chip. 2005;5(11):1233-9.
12. Petersson F, Åberg L, Swärd-Nilsson AM, Laurell T. Free flow acoustophoresis: microfluidic-based mode of particle and cell separation. Analytical chemistry. 2007 Jul 15;79(14):5117-23.
13. Laurell T, Petersson F, Nilsson A. Chip integrated strategies for acoustic separation and manipulation of cells and particles. Chemical Society Reviews. 2007;36(3):492-506.
14. Augustsson P, Magnusson C, Nordin M, Lilja H, Laurell T. Microfluidic, label-free enrichment of prostate cancer cells in blood based on acoustophoresis. Analytical chemistry. 2012 Aug 28;84(18):7954-62.
15. Lenshof A, Magnusson C, Laurell T. Acoustofluidics 8: Applications of acoustophoresis in continuous flow microsystems. Lab on a Chip. 2012;12(7):1210-23.
16. Antfolk M, Antfolk C, Lilja H, Laurell T, Augustsson P. A single inlet two-stage acoustophoresis chip enabling tumor cell enrichment from white blood cells. Lab on a chip. 2015;15(9):2102-9.

17. Dykes J, Lenshof A, Åstrand-Grundström B, Laurell T, Scheding S. Efficient removal of platelets from peripheral blood progenitor cell products using a novel micro-chip based acoustophoretic platform. PloS one. 2011 Aug 9;6(8):e23074.
18. Evander M, Johansson L, Lilliehorn T, Piskur J, Lindvall M, Johansson S, Almqvist M, Laurell T, Nilsson J. Noninvasive acoustic cell trapping in a microfluidic perfusion system for online bioassays. Analytical chemistry. 2007 Apr 1;79(7):2984-91.
19. Thévoz P, Adams JD, Shea H, Bruus H, Soh HT. Acoustophoretic synchronization of mammalian cells in microchannels. Analytical chemistry. 2010 Mar 3;82(7):3094-8.
20. Yang AH, Soh HT. Acoustophoretic sorting of viable mammalian cells in a microfluidic device. Analytical chemistry. 2012 Dec 6;84(24):10756-62.
21. Yang T, Bragheri F, Nava G, Chiodi I, Mondello C, Osellame R, Berg-Sørensen K, Cristiani I, Minzioni P. A comprehensive strategy for the analysis of acoustic compressibility and optical deformability on single cells. Scientific reports. 2016 Apr 4;6:23946.
22. Huang PH, Ren L, Nama N, Li S, Li P, Yao X, Cuento RA, Wei CH, Chen Y, Xie Y, Nawaz AA. An acoustofluidic sputum liquefier. Lab on a Chip. 2015;15(15):3125-31.
23. Goddard G, Martin JC, Graves SW, Kaduchak G. Ultrasonic particle- concentration for sheathless focusing of particles for analysis in a flow cytometer. Cytometry Part A: The Journal of the International Society for Analytical Cytology. 2006 Feb;69(2):66-74.

24. Goddard GR, Sanders CK, Martin JC, Kaduchak G, Graves SW. Analytical performance of an ultrasonic particle focusing flow cytometer. Analytical chemistry. 2007 Nov 15;79(22):8740-6.
25. Wiklund M, Günther C, Lemor R, Jäger M, Fuhr G, Hertz HM. Ultrasonic standing wave manipulation technology integrated into a dielectrophoretic chip. Lab on a Chip. 2006;6(12):1537-44.
26. Kim SH, Antfolk M, Kobayashi M, Kaneda S, Laurell T, Fujii T. Highly efficient single cell arraying by integrating acoustophoretic cell pre-concentration and dielectrophoretic cell trapping. Lab on a Chip. 2015;15(22):4356-63.
27. Destgeer G, Cho H, Ha BH, Jung JH, Park J, Sung HJ. Acoustofluidic particle manipulation inside a sessile droplet: four distinct regimes of particle concentration. Lab on a Chip. 2016;16(4):660-7.
28. Fornell A, Nilsson J, Jonsson L, Periyannan Rajeswari PK, Joensson HN, Tenje M. Controlled lateral positioning of microparticles inside droplets using acoustophoresis. Analytical chemistry. 2015 Oct 9;87(20):10521-6.
29. Cesewski E, Haring AP, Tong Y, Singh M, Thakur R, Laheri S, Read KA, Powell MD, Oestreich KJ, Johnson BN. Additive manufacturing of three-dimensional (3D) microfluidic-based microelectromechanical systems (MEMS) for acoustofluidic applications. Lab on a Chip. 2018;18(14):2087-98.
30. Dual J, Leibacher I, Reichert P, inventors; Eidgenoessische Technische Hochschule Zurich (ETHZ), assignee. Acoustophoretic droplet handling in bulk acoustic wave devices. United States patent application US 15/111,854. 2016 Nov 17.

31. Wu M, Ouyang Y, Wang Z, Zhang R, Huang PH, Chen C, Li H, Li P, Quinn D, Dao M, Suresh S. Isolation of exosomes from whole blood by integrating acoustics and microfluidics. Proceedings of the National Academy of Sciences. 2017 Oct 3;114(40):10584-9.
32. Shi J, Huang H, Stratton Z, Huang Y, Huang TJ. Continuous particle separation in a microfluidic channel via standing surface acoustic waves (SSAW). Lab on a Chip. 2009;9(23):3354-9.
33. Lenshof A, Evander M, Laurell T, Nilsson J. Acoustofluidics 5: Building microfluidic acoustic resonators. Lab on a Chip. 2012;12(4):684-95.
34. Hawkes JJ, Coakley WT. Force field particle filter, combining ultrasound standing waves and laminar flow. Sensors and Actuators B: Chemical. 2001 May 15;75(3):213-22.
35. Wu M, Ozcelik A, Rufo J, Wang Z, Fang R, Huang TJ. Acoustofluidic separation of cells and particles. Microsystems & nanoengineering. 2019 Jun 3;5(1):32.
36. Zhao Z, Yang Y, Zeng Y, He M. A microfluidic ExoSearch chip for multiplexed exosome detection towards blood-based ovarian cancer diagnosis. Lab on a Chip. 2016;16(3):489-96.
37. Ibsen SD, Wright J, Lewis JM, Kim S, Ko SY, Ong J, Manouchehri S, Vyas A, Akers J, Chen CC, Carter BS. Rapid isolation and detection of exosomes and associated biomarkers from plasma. ACS nano. 2017 Jul 3;11(7):6641-51.

38. Wang Z, Wu HJ, Fine D, Schmulen J, Hu Y, Godin B, Zhang JX, Liu X. Ciliated micropillars for the microfluidic-based isolation of nanoscale lipid vesicles. Lab on a Chip. 2013;13(15):2879-82.
39. Wunsch BH, Smith JT, Gifford SM, Wang C, Brink M, Bruce RL, Austin RH, Stolovitzky G, Astier Y. Nanoscale lateral displacement arrays for the separation of exosomes and colloids down to 20 nm. Nature nanotechnology. 2016 Nov;11(11):936.
40. Streets AM, Huang Y. Chip in a lab: Microfluidics for next generation life science research. Biomicrofluidics. 2013 Jan 31;7(1):011302.
41. Dual J, Hahn P, Leibacher I, Möller D, Schwarz T. Acoustofluidics 6: Experimental characterization of ultrasonic particle manipulation devices. Lab on a Chip. 2012;12(5):852-62.
42. Teh SY, Lin R, Hung LH, Lee AP. Droplet microfluidics. Lab on a Chip. 2008;8(2):198-220.

2. ACOUSTOFLUIDIC MICRODEVICE FOR ROBUST CONTROL OF PRESSURE NODAL POSITIONS

2.1. Introduction

To date a variety of particle and cell manipulation applications have been developed using bulk acoustic wave (BAW)-based acoustofluidic systems. The principle of those systems lies on the phenomena that particles passing through an acoustic resonance field, namely acoustic standing wave created between two side channels of a microfluidic channel functioning as half-wavelength resonators, move towards positions in the microfluidic channel called acoustic pressure nodes and/or anti-nodes, depending on their acoustic contrast factor. Depending on the frequency applied through the piezoelectric transducer generating the acoustic wave, these acoustic pressure nodes are generated in the ½ position, ¼ and ¾ positions, and so on of the microfluidic channel width. The major benefits of bulk acoustofluidic technology is that it can provide contactless and label-free manipulation of particles, including cells, in microscale with extremely simple microstructures and instrument setup. Thanks to these benefits, this technology has been widely used in applications ranging from cell separation [1, 2], oil droplet separation [3], cell property analysis [4, 5, 6], and cell trapping [7]. Additionally, this technology has been combined with other available microfluidic technologies, such as droplet microfluidics [8, 9] and electrophoresis [10], for more complex assays to be performed in microfluidic format.

To actuate bulk acoustofluidic microdevices, a piezoelectric transducer typically attached to the backside of a microfluidic channel is excited at the resonant frequency that matches the acoustic wavelength of the width of the microchannel. At this resonant frequency, particles passing through the acoustic resonance field move towards the acoustic pressure nodes or anti-nodes based on their density and compressibility in comparison to those properties of the surrounding media. If the particles have a positive acoustic contrast factor, they move towards the acoustic pressure node where the amplitude of motion is zero. On the other hand, if particles have a negative acoustic contrast factor, they move towards the acoustic pressure anti-node where the amplitude of motion is maximum. This allows particle and cell manipulation to be conducted very easily. However, one of the biggest limitations of this technology is that the location of the acoustic pressure nodes is fixed, in a sense that they can only be formed at the ½ (primary) or ¼ & ¾ (secondary) positions (or even 1/6 in the case of tertiary pressure nodes, but not commonly used as the force is significantly weaker) in a given microfluidic channel when the primary, secondary, and tertiary acoustic resonance frequencies are applied. Thus, this technology cannot be used to manipulate cells and particles to any position desired within a microfluidic channel, thus somewhat limiting its flexibility and application areas. More flexible capability in controlling the location of the acoustic nodal positions will enable changing the location of particles and cells inside a microchannel more freely, and make applications that require better control over the location of particles and cells in a given microchannel easier to be implemented.

The possibility of moving particles to a position other than the fixed acoustic nodal lines through decoupling the physical microfluidic boundary from the acoustic wave boundary has been demonstrated [11]. In that study, an acoustically transparent thin sidewall was created within the silicon microfluidic channel by filling part of the microfluidic channel with a polydimethyl siloxane (PDMS) structure, removed by laser cutting, so that the fluidic boundary created by the PDMS sidewall could be decoupled from the acoustic boundary created by the silicon microfluidic channel sidewall. This was possible because PDMS is relatively transparent to acoustic wave. By adjusting the width of this PDMS structure inside the silicon microfluidic channel, the effective position of the acoustic nodal position could be adjusted within the flow channel, where the actual acoustic nodal position is fixed by the two sidewalls of the silicon microchannel but the microfluidic channel width is reduced by the width of the PDMS structure within the microfluidic channel. Another reported method is the use of a bypass channel (so-called echo-channel) adjacent to the main flow channel that allowed the acoustic pressure nodes and anti-nodes to be dynamically tuned depending on what medium is filling the echo-channel [12]. Here, the main flow channel was physically separated from the echo-channel by a thin side wall (less than 20 μm in width), at the same time being almost transparent to the acoustic wave. Thus, the combined width of the main channel and the echo-channel becomes the effective channel width, while the flow channel is defined by walls of the main flow channel. By filling this echo-channel with medium having different densities, and thus changing the speed of sound wave, it was possible to create an acoustic pressure node in any location within the main channel. Although overcoming many limitations of

conventional bulk acoustofluidics, changing the location of cells and particles along the flow direction of the channel is still not possible, as the locations of the acoustic pressure nodes are still fixed and cannot change along the flow direction of a microfluidic channel.

Here, we present a bulk acoustofluidic device where the echo-channel has different widths along the flow direction of the main channel, essentially changing the effective acoustofluidic channel width along the flow direction. This allows the position of the acoustic pressure node to change along the flow direction, enabling the location of particles and cells to change laterally as they flow through the main flow channel. This new method provides the first bulk acoustofluidic method that allows the position of particles and cells to change laterally as they move along the flow direction and has the potential to further broaden the application areas of bulk acoustofluidics.

2.2. Materials and Methods

2.2.1. Microdevice Fabrication

The acoustofluidic microdevices were fabricated by the following steps. First, the microfluidic channel designs were patterned by photolithography on a Si wafer and then etched into the silicon substrates using deep reactive ion etching (DRIE) to a depth of 105 µm. Fluidic access holes were drilled in a 500 µm thick borosilicate glass layer using a diamond-plated drill bit mounted on a benchtop drill press (DP101, Ryobi Ltd, SC). The glass and silicon layer were anodically bonded at 400 °C by applying 700 V of DC voltage for 40 min. After the bonding process, ferrules were glued onto the holes of the glass layer using epoxy for fluidic access. Tygon tubings (VWR, PA, USA) were inserted inside the

ferrules and sealed with epoxy. The PZ26 type PZT (Ferroperm, Denmark) was bonded to the bottom of the chip with cyanoacrylic glue (Loctite, USA), and wires were soldered to the PZT for electrical interconnect.

2.2.2. Acoustofluidic Device Testing

Acoustofluidic device testing was conducted under an upright microscope (Eclipse LV100D, Nikon Inc, Japan) and fluids were flown through the microchannels by a 4-barrel syringe pump (Fusion 400, Chemyx Inc, MA). The flow rate was chosen to be 500 μL/h. Fluorescent polystyrene microspheres (Thermoscientific, CA, USA) mixed with de-ionized (DI) water was used for all experiments for easy visualization of particle movement. For devices with the straight echo-channel design (single width throughout the length of the microchannel), a function generator (DG4202, Rigol Technologies Inc, USA) was utilized to generate a sinusoidal signal that was amplified through a 50-dB power amplifier (2100L, E&I, Ltd.) and applied to the PZT. For the chip with changing echo-channel width, a LabVIEW™ (National Instruments, TX) program was developed to generate sums of two sinusoidal signals from a function generator (AFG3021B, Tektronix Inc, USA). This signal was then applied to the PZT through a 50-dB power amplifier (2100L, E&I, Ltd.).

2.2.3. Working Principle

In wave theory, wavelength equals to the speed of wave times the frequency of the wave. In acoustofluidics, if the wavelength of the acoustic wave is adjusted to be equal to

the microchannel width or multiples of the channel width, an acoustic resonance field is generated. If the channel width is equal to half of the acoustic wavelength, it means that the channel is in its first harmonic ($\lambda/2$) mode, and there will be one nodal plane created in the middle of the microchannel. Similarly, if the channel width is equal to the wavelength, the channel is in its second harmonic (λ) mode, and in this case, there will be two pressure nodal planes, one at the ¼ position and the other at the ¾ position within the channel (**Fig. 2.1A**).

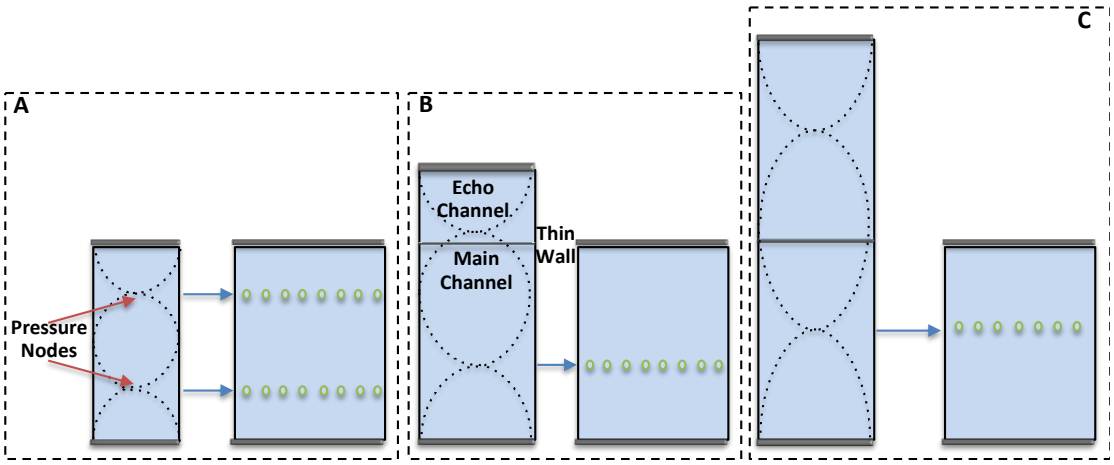

Figure 2.1 Effect of Echo-channel on Acoustic Pressure Nodal Positions when there is no echo-channel **(A)**, a narrow echo-channel separated by a thin wall **(B)**, and on a wide echo-channel **(C)** excited at the second harmonic mode.

If an echo-channel is added next to the main fluidic channel separated by a thin wall, the thin wall functions as a physical boundary for the flow itself but almost transparent to the acoustic wave. This makes the width of the combined main channel and the echo-channel as the effective channel width of acoustic full wavelength resonator. Thus, from acoustofluidics perspective, the effective channel width W_{eff} can be defined as

the following equation (1), which can be used to calculate the needed resonance frequency [13].

$$W_{eff} = W_{main} + W_{echo}\,(C_w/C_{echo}) + T_{wall}\,(C_w/C_{Si}) \qquad (6)$$

In this equation, W_{eff} stands for the effective channel width from acoustic wave perspective and as being the sum of the main channel width, W_{main}, and the scaled version of the echo-channel width, W_{echo}, and the scaled version of the thickness of the wall that separates the echo-channel and the main channel, T_{wall}. C_w is the speed of sound in the main flow channel and set as 1531 m/s [14]. C_{echo} is the speed of sound inside the echo-channel and set as 1496 m/s since deionized (DI) water was used in the echo-channel [15]. C_{Si} represents the speed of sound in silicon and the value was set to 8433 m/s [16]. The resonant frequency in the second harmonic mode was represented as $\boldsymbol{f_1}$ and calculated by dividing the speed of sound in the microfluidic channel by the effective channel width. COMSOL Multiphysics™ software was utilized to examine the effect of echo-channel width on the positions of acoustic pressure nodes.

As shown in **Fig. 2.1** echo-channel which is adjacent to main microfluidic channel helps changing the acoustic pressure nodal positions in the main fluidic channel. When the width of the echo-channel increases, the effective channel width also increases, which causes the nodal positions on the main channel to shift towards the echo-channel. If this device is actuated in its second harmonic ($\boldsymbol{\lambda}$) mode, there will be two acoustic pressure nodal planes. However, the location of those planes can be adjusted using the echo-

channel so that one nodal plane is formed inside the main fluidic channel and the other one formed inside the echo-channel, resulting in only one pressure nodal plane to exist in the main flow channel. This phenomenon is very convenient since it is not desired to have two nodal planes resulting in particles or cells moving to two different locations inside the flow channel.

Devices with different main channel and echo-channel widths were tested to fully characterize this concept. In the first design, the main channel width was 1600 micrometer (μm) and the echo-channel widths varied from 678 μm to 2678 μm, giving an expected acoustic resonance frequency ranging between 350 kilohertz (kHz) and 660 kHz. In the second set of designs, the main channel width was reduced to 800 μm to increase the frequency range to be tuned between 840 kHz and 1.31 megahertz (MHz) to avoid possible overlapping of the resonant frequencies. For example, when the echo-channel width is 1078 μm, the expected resonant frequency is 0.56 MHz, which is very close to 0.55 MHz, which is the resonant frequency when the echo-channel width is 1478 μm. Finally, an echo-channel where the width changed from 1800 to 1000 and then to 300 μm like a staircase along the flow direction was designed. In this design, the wall thickness was increased to 20 μm to avoid potential leakage issue between the two adjacent channels.

2.3. Results

2.3.1. Straight Echo-Channel Devices

We first attempted to determine whether the acoustic pressure and anti-pressure nodal positions could be successfully changed in the microfluidic channel of the

acoustofluidic chip. For that purpose, COMSOL simulations were run by using different channel geometry values. As seen in **Fig 2.2A** straight echo-channel device was modeled in xy-plane (2-D) and in the model silicon material is assigned to the middle layer and water is assigned to main and echo-channel. Following that the model was divided into smaller elements using the mesh function (**Fig. 2.2B**). In one of the simulation models main channel width is kept at 800 μm and the echo-channel width is increased from 343 μm to 975 μm.

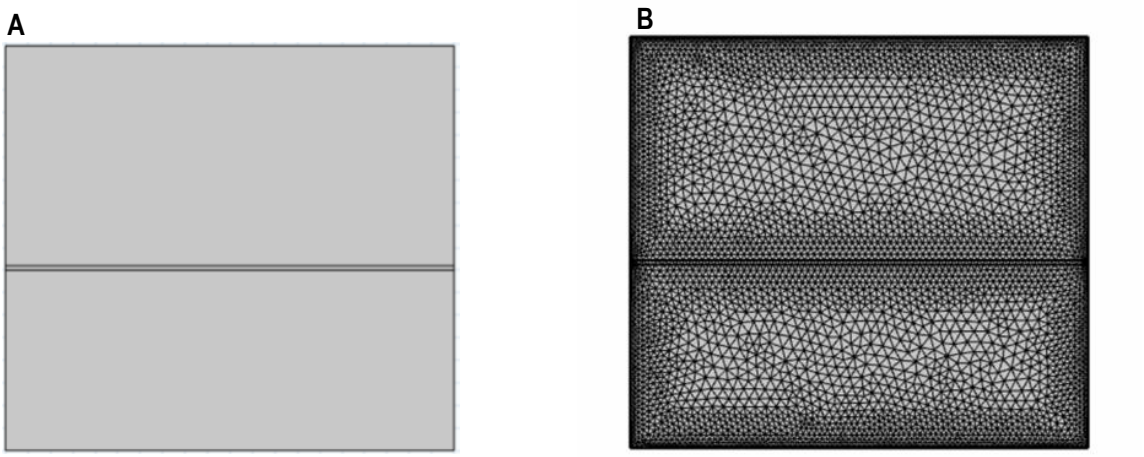

Figure 2.2 A. 2-D model in COMSOL when main channel width is 800 and echo-channel width is 975 μm **B**. Model after using the mesh function in COMSOL model

As shown in **Fig 2.3** of FEA simulation results, the position of acoustic pressure node can be moved closer to the thin wall between two microfluidic channels by increasing the echo-channel width from 343 μm to 975 μm. By doing so the second acoustic pressure nodal plane in the upper stream can be moved to the echo-channel and by taking advantage of lower nodal plane particle/cell manipulation can be done effectively.

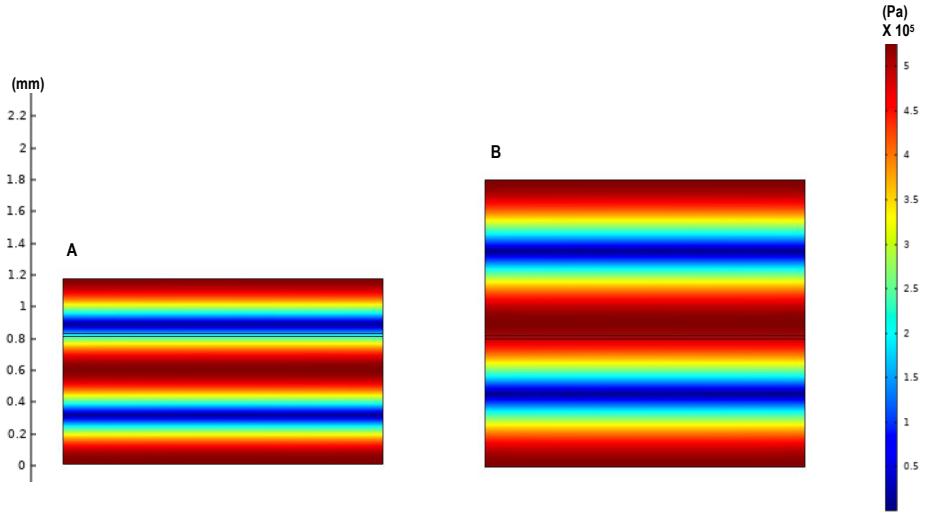

Figure 2.3 A. Acoustic pressure along the channel width when main channel width is 800 and echo channel width is 343 µm and applied frequency is 1.31 MHz, **B**. Acoustic Pressure when echo channel width is 975 µm and applied frequency is 0.84 MHz

Following that, two types of acoustofluidic devices were tested. In the first set of chips, the main channel width was selected to be 1600 µm and the wall thickness was microfabricated to be 10 µm. For reference one of the fabricated acoustofluidic chips is shown in **Fig. 2.4** after anodic bonding and device packaging.

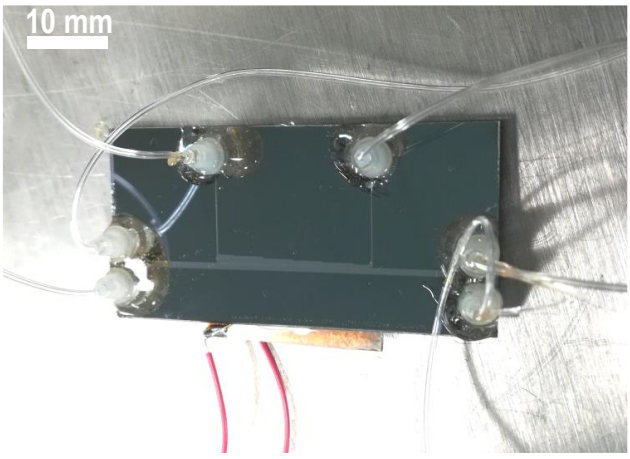

Figure 2.4 Image of one of the fabricated acoustofluidic chips with echo-channels with changing widths.

To minimize the potential overlaps in the resonant frequencies the channel width was reduced in the second design by making the main channel width to 800 μm so that by the frequency range was broadened. **Fig. 2.5** shows the scanning electron microscopy (SEM) image of the fabricated acoustofluidic chip with straight echo-channel.

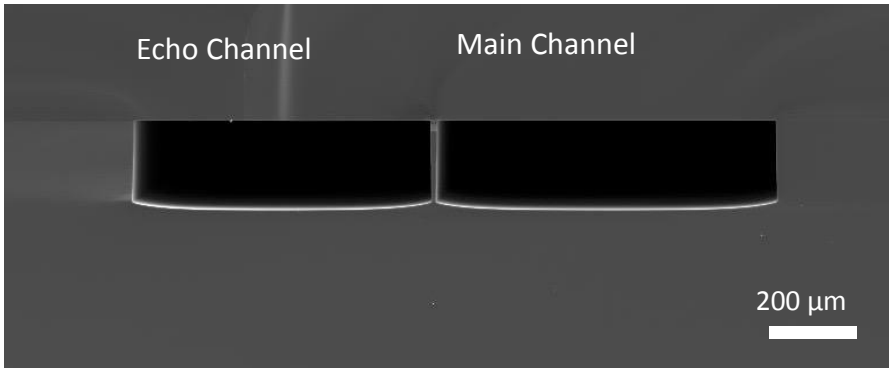

Figure 2.5 Cross-sectional SEM image of the anodically bonded acoustofluidic device with echo-channel.

As seen in **Fig 2.6A** location of focused polystyrene microspheres is ~302 μm far from the lower acoustic boundary of the chip, when the main channel width is 800 μm and the echo-channel width is 450 μm. In this experimental scenario, the frequency of the sinusoidal signal applied to the PZT was 1.26 MHz and V_{pp} was set to 120 mV at the ends of the power amplifier. When echo-channel width is equal to 975 μm the location for acoustic pressure nodal position becomes ~426 μm far from the lower wall (**Fig 2.6B**). To actuate this chip, the frequency of applied signal was 0.83 MHz and V_{pp} was 180 mV. It required slightly more voltage when compared to the chip with 450 μm-wide echo-channel since the impedance of the PZT changes with the frequency.

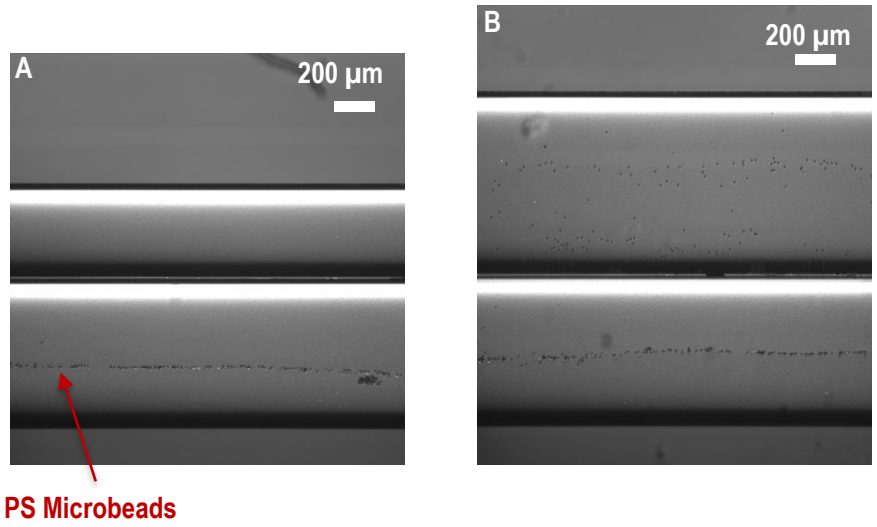

Figure 2.6 Representative brightfield (BF) microscopic image (exposure time: 10 ms) that shows the nodal plane positions to which particles are focused (f1:1.26 MHz, Vpp:120 mV, flow rate: 500 µl/h) when using a 450 µm wide echo-channel **(A)** Representative BF microscopic image (exposure time: 10 ms) that shows the nodal plane position to which particles are focused (f1:0.83 MHz, Vpp:180 mV, flow rate: 500 µl/h) when using a 975 µm wide echo-channel **(B).**

As the echo-channel becomes wider, it can be seen that the particle position successfully changes from the 527 µm position to the 921 µm position (**Fig. 2.7**).

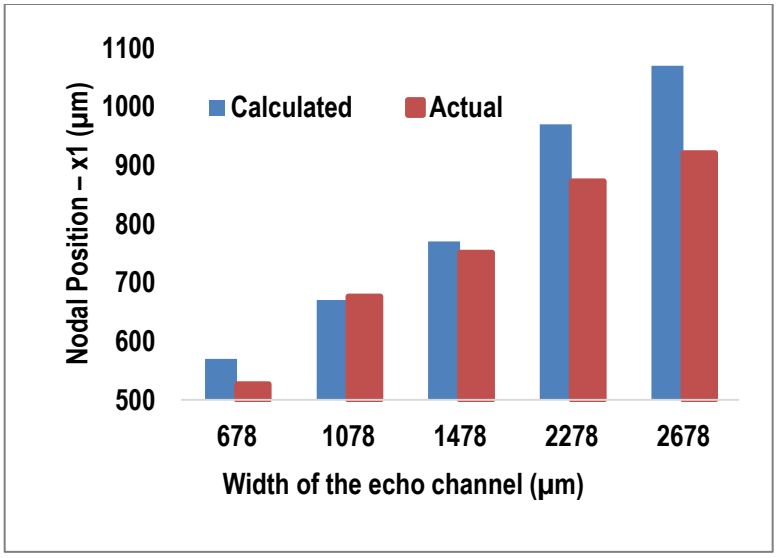

Figure 2.7 Graph of the expected and actual nodal positions (main channel widths are 1600 µm).

At the same time, it can also be seen that as the echo-channel becomes wider, the discrepancy between the calculated nodal position and actual nodal position becomes larger. The resonance frequency required to focus particles to the nodal position has about 7% difference compared to the calculated value (**Fig. 2.8**).

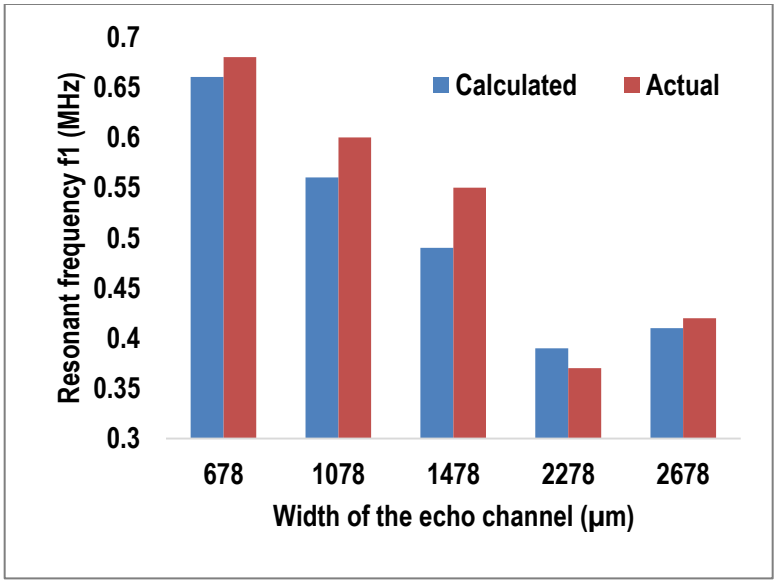

Figure 2.8 A graph of the expected and actual resonant frequencies (main channel widths are 1600 µm).

In **Table 2.1** all the results of experiments done with first set of chips such as expected and actual nodal positions and frequencies were summarized. Also, the minimum required voltages to focus the microparticles to the nodal positions in each device were added to the table. Referring to the table as the echo-channel width increases the frequency range to be applied to focus the microparticles gets narrower, and this narrow frequency range causes mismatching of resonant frequencies.

Table 2.1 Summary of the various echo-channels and corresponding parameters tested. In all cases, the width of the main channel is 1600 μm and wall thickness is 10 μm.

Main Channel Characteristics (μm)					**Calc. Freq (MHz)**	**Real Freq (MHz) & Vpp**
W_{main}	W_{echo}	W_{eff}	**Calc.** x_1	**Real** x_1	f_1	f_1
1600	678	2280	570	527±12	0.66	0.68 & 130 mV
1600	1078	2680	670	676±17	0.56	0.60 & 460 mV
1600	1478	3080	770	751±15	0.49	0.55 & 64 mV
1600	2278	3880	970	873±22	0.39	0.37 & 400 mV
1600	2678	4280	1070	921±18	0.35	0.42 & 400 mV

For instance; when echo-channel widths are 2678 μm, applied frequency is 20% off from the expected result. It was realized that the frequency range should be broadened so that overlapping of corresponding frequencies for different echo-channel widths could be avoided. Out of those first set of chips when echo-channel widths are smaller than 1478 μm the discrepancy between the expected and actual nodal positions was less than 50 μm.

However, for larger echo-channel widths like 2278 and 2678 μm the discrepancy is much bigger as shown in **Table 2.1**.

To assess the knowledge how different channel widths, affect the control of the particle focusing position, the main channel widths of 800 μm and 1600 μm with different echo-channel widths were tested. As shown in **Table 2.1**, range of frequency to be tuned to generate acoustic resonance for chips with 1600 μm-wide main channels is relatively narrow when compared to 800 μm-wide main channel devices. Since shrinking the channel widths will require higher frequency, the range of tuned frequency for 800 μm-wide devices is much wider when compared to the first set of devices. Therefore, second set of devices provided better divergence to the calculated values as seen in **Table 2.2**.

Table 2.2 Summary of the various echo-channels and corresponding parameters tested. In all cases, the width of the main channel is 800 μm and the wall thickness is 10 μm.

Main Channel Characteristics (μm)					**Calc. Freq (MHz)**	**Real Freq (MHz) & Vpp**
W_{main}	W_{echo}	W_{eff}	***Calc.*** x_1	***Real*** x_1	f_1	f_1
800	975	1787	447	426 ± 11	0.84	0.83 &180 mV
800	785	1595	399	402±8	0.94	0.94 &250mV
800	605	1413	353	364±5	1.06	1.06 &370mV
800	450	1257	314	302±4	1.20	1.26 &120mV
800	343	1148	287	276±3	1.31	1.42&180 mV

For instance, increasing the echo-channel width from 450 μm to 605 μm will almost results ~70 μm change on the acoustic pressure nodal plane. **Fig. 2.9** shows the brightfield images of different particle positions for varying echo-channel widths when main channel width is kept at 800 μm.

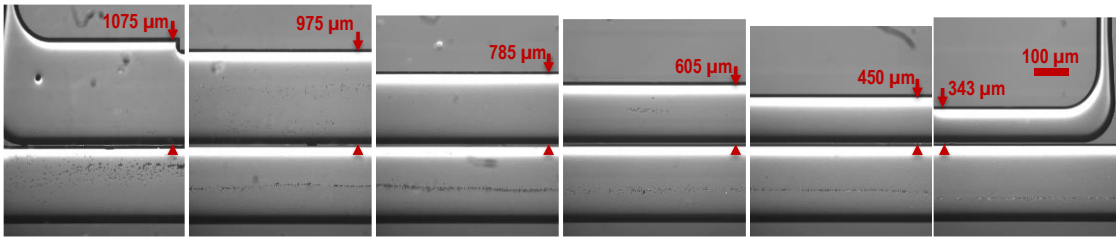

Figure 2.9 Bright field microscopic images (exposure time: 10 ms) showing particle positions within the main channel when the echo-channel width changes from 1075 µm to 343 µm.

In the case of echo-channel width is equal to 1075 µm successful focusing of polystyrene microspheres could not be implemented. However, for other echo-channel width designs the particle migration to acoustic pressure nodes were successfully demonstrated. **Table 2.2** summarizes the calculated and experimental resonant frequencies for different echo-channels. When echo-channel width is equal to 450 µm the minimum peak-peak voltage required to focus the microspheres successfully at one nodal plane is 120 mV and resonant frequency is 1.26 MHz. When compared to the other echo-channels the impedance of the PZT at that frequency is lower so that successful migration of microparticles to nodal plane for 450 µm wide echo-channel can be seen in **Fig. 2.10**. Changing echo-channel from 975 µm to 343 µm when main channel width is kept at 800 µm makes the acoustic pressure nodal position change from ~426 µm to ~376 µm as shown in same figure**,**.

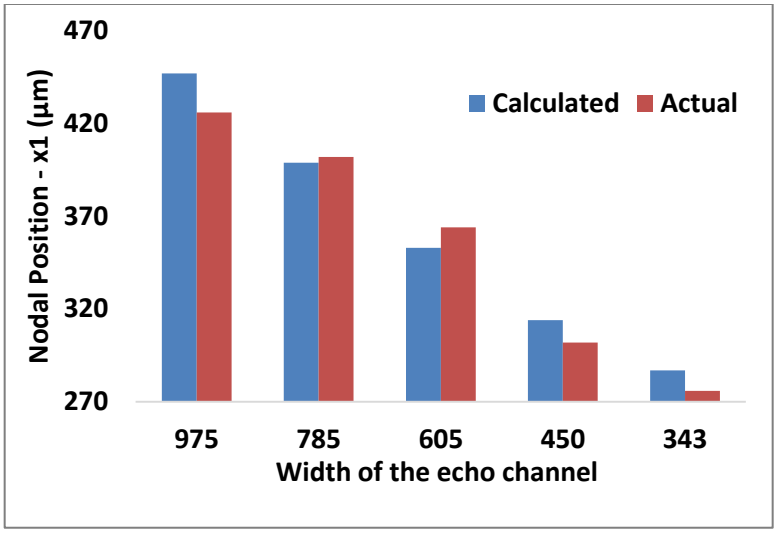

Figure 2.10 A graph to show expected and actual nodal positions**.**

Expected and real resonant frequencies are very close when the main channel width and the echo-channel width values are close to each other. For instance, when echo-channel widths are 605 and 785 µm the expected and real resonant frequencies are equal to each other as seen in **Fig 2.11**. However, when echo-channel width is much bigger or smaller than the main channel width expected resonant frequency and real resonant frequency values have some discrepancy.

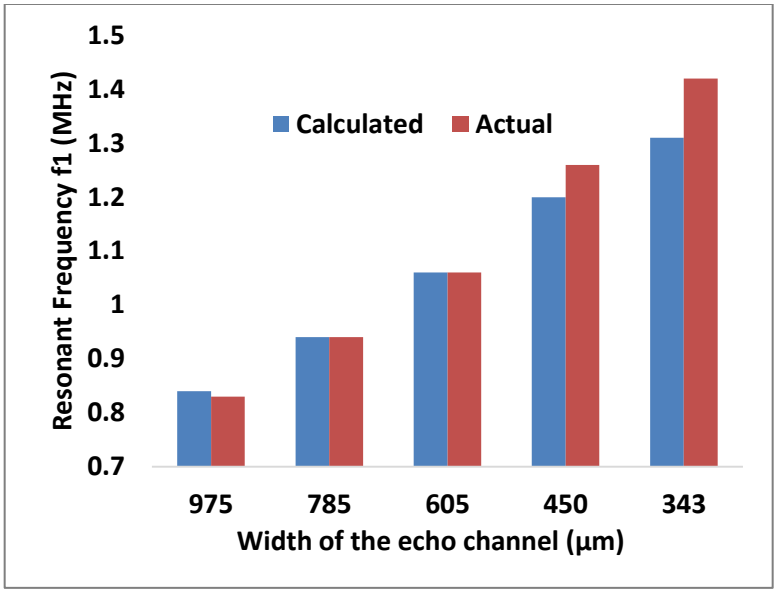

Figure 2.11 A graph to show expected and actual nodal positions.

While trying to change acoustic pressure nodal/anti-nodal planes by exploiting the idea of adding an echo-channel adjacent to main fluidic channel some limitations arose. First limitation was the geometry of the microfluidic chips. Since the main fluidic channel was separated from the echo-channel by a thin wall one of the nodal positions has to be located in the echo-channel so that acoustic pressure nodal position inside the main fluidic channel could be adjusted. This adjustment could be implemented by making the echo-channel width one third of the main channel width as minimum or three times of the main channel width as maximum. Doing so kept one of the nodal positions inside the main fluidic channel and will keep the other one inside the echo-channel. By considering that the wall thickness should be kept at minimum to reduce the loss while acoustic waves travel between the acoustic boundaries while avoiding the leakage between two microfluidic channels. In some regions of the first two set of devices, particle flow was

observed in the echo-channel where normally no particles should flow. The reason of that was considered because of the wall thickness being 10 μm and in some regions of this wall the bonding between the silicon channel and glass was not successful during the anoding bonding process.

Besides that, as seen from **Table 2.1** and **Table 2.2** there are some discrepancies between the expected and the actual values. There can be multiple reasons why there is a discrepancy between the calculated nodal position and the real nodal position observed. One of the reasons could be the wall thickness between the main fluidic channel and the echo-channel. Another reason could be mismatching between the acoustic resonance frequency and the resonant frequency of PZT.

Most importantly, the calculation does not account for the requirement of the voltage level to successfully move particles to the nodal positions. Different level of voltage applied may have different effect on the thin side wall, and thus may affect the nodal position. Increased temperature level due to higher voltage applied can also affect the nodal position. Even though a cooling fan was somewhat successfully employed to limit the rise in temperature, any voltage beyond about 300 mV (applied to the amplifier) resulted in at least 20 °C increase in temperature, which affect the sound velocity, thus the actual acoustic pressure nodal position.

Second, this discrepancy may be also attributed to the PZT transducer characteristics. PZT has its intrinsic electrical impedance, which is highly dependent on the applied frequency. The frequency at which the discrepancy between calculation and actual result is minimum (for 878 and 2678-μm wide echo-channels), those frequencies

were in line with reported resonant frequencies of the PZT we used in our experiment. If the driving frequency is away from this PZT resonance frequency, a higher voltage will be required to overcome the impedance of the transducer, thus affecting the nodal position as described in the previous paragraph. As summarized in **Table 2.1** and **Table 2.2** at some frequencies the PZT needed higher voltage to actuate the acoustofluidic chip when compared to the other frequencies. This shows that impedance of PZT might affect the acoustic actuation in a good or bad way. If the impedance of the transducer is small at that frequency with very low voltage actuation can be realized. On the other hand, if the impedance of the transducer is high at certain frequency resonance will need higher voltage for actuation.

2.3.2. Staircase Echo-Channel Device

After the experiments with straight echo-channel devices it was realized that as driving frequency changes the electrical impedance of the PZT varies and that impedance has a significant impact on the acoustophoretic force since voltage required to focus microparticles is a factor on acoustophoretic force. For instance, while testing one of the 1600 μm devices the applied frequency to the PZT is equal to 0.6 MHz and the peak-peak voltage required to focus the microbeads was 460 mV in this case as being much higher than the voltage needed at 0.55 MHz where echo-channel width is 1478 μm as shown in **Table 2.1**. Similarly, when the applied frequency is 1.06 MHz required peak-peak voltage was 370 mV which is almost three times of the voltage required to focus the microbeads when applied frequency is 1.26 MHz. This phenomenon shows that required voltage to

generate acoustic resonance is strictly dependent on the applied frequency and the impedance of the PZT since it was shown that electrical impedance of the PZT is dependent on the frequency [17]. To be able to generate acoustic resonance without applying too high of a power that causes overheating issue, it is essential to overcome the impedance of the PZT with relatively low voltage.

By taking this into account, a third design was created where the main channel width was 700 μm, so that the frequencies of 420 kHz and 1.06 MHz with higher impedances were tried to be avoided. Additionally, echo-channel widths through the chip varied to change the nodal positions in a single acoustofluidic chip. Based on the relationship between the echo-channel and the actual nodal position of the microparticles, a microchannel that has a staircase echo-channel composed of 3 different steps (i.e., echo-channel width) was designed (**Fig. 2.12**).

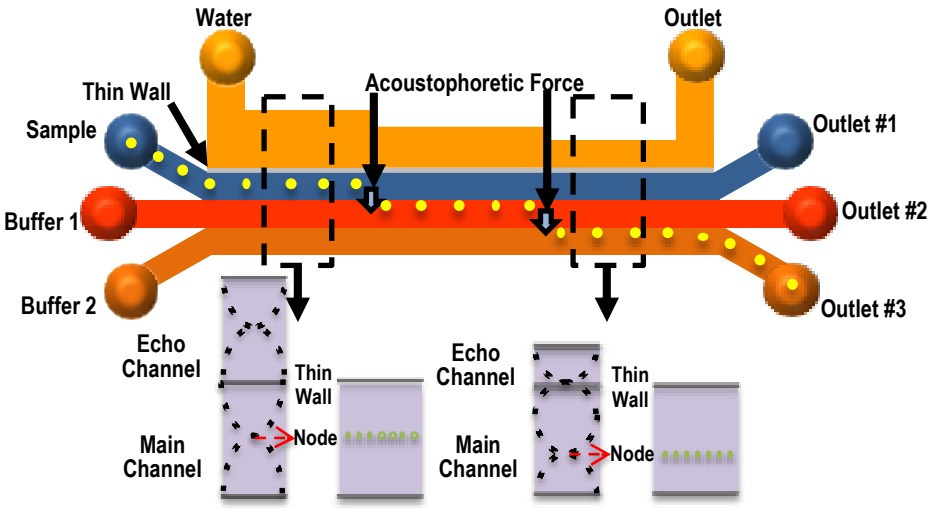

Figure 2.12 Illustration of the 3-step staircase echo-channel acoustofluidic device.

To make particle manipulation at high frequency, the resonant frequency of PZ26 type-PZT, which is ~2 MHz, was considered. Based on the PZT impedance report from the vendor, the frequency values where impedance is relatively low such as 1.49 MHz, 0.88 MHz, and 0.60 MHz were chosen as reference point to design the staircase echo-channel device. Based on those results, an acoustic microfluidic chip with a staircase echo-channel was designed so that the resonant frequencies could be applied as sum of sinusoidal signals without requiring the dynamical change of frequency and applied voltage. By considering these design parameters, the main channel width was reduced to 700 μm and echo-channel widths are calculated using those frequency values as shown in **Table 2.3**. As seen from the table frequency values while testing this chip are very close to expected frequency values to run the PZT. Furthermore, the nodal position change is ~280 μm which is almost 40% of the main channel width.

Table 2.3 Table for staircase echo-channel device when width of the main channel is 700 μm and wall thickness is 20 μm for different echo-channel widths

Main Channel Characteristics (μm)					**Calc. Freq (MHz)**	**Real Freq (MHz) & Vpp**
W_{main}	W_{echo}	W_{eff}	**Calc.** x_1	**Real** x_1	f_1	f_1
700	300	1004	251	356±4	1.49	1.50 ± 0.01 & (350mV)
700	1000	1704	426	425±4	0.88	0.89 ± 0.01 & (230mV)

700	1800	2504	626	638±5	0.60	0.61 ± 0.03 & (800mV)

When compared to obtained data from straight echo-channel devices even though nodal position change for 1600 μm-wide chips is ~394 μm as being less than %25 of the main channel width, 700 μm-wide devices have better capability in terms of nodal position change as percentage of main channel width. As seen from **Fig. 2.13**, fluorescent microparticles were descended into the acoustic pressure nodes by reducing the echo-channel width along with the flow direction. Again, the reason for discrepancy between the real nodal position and expected one could be because of overheating of the PZT during the actuation process.

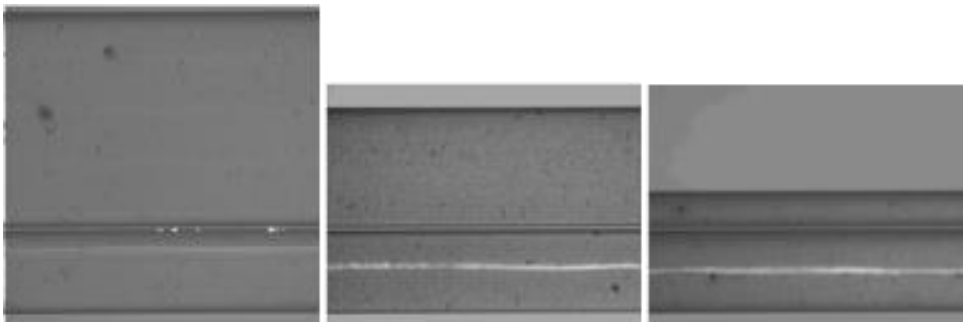

Figure 2.13 Microscope images showing fluorescent PS particles being focused to different pressure node positions when the echo-channel widths are 1800, 1000, and 300 μm (from left to right). Bright field images (10 ms exposure time) showing the microchannels were overlaid with fluorescent images (400 ms exposure time) showing fluorescent microbeads to make visualization easy.

Even though the frequency values match with the expected values as seen from **Fig. 2.14** for 700 μm-wide chip, the nodal position for 300 μm-wide channel has a bigger variance compared to the other steps.

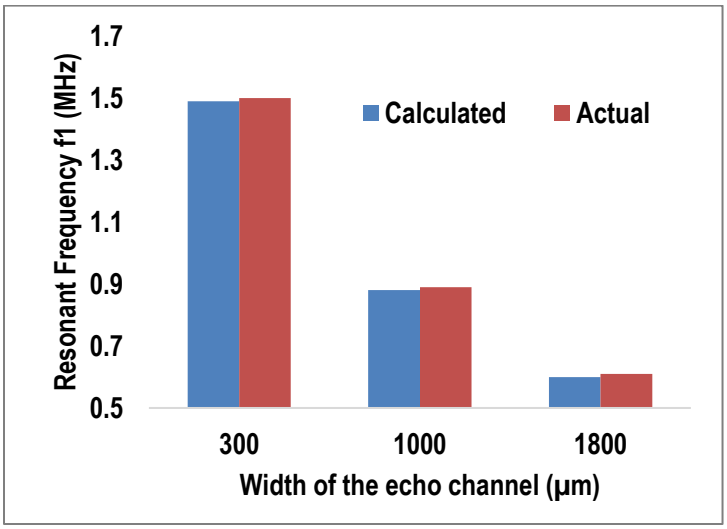

Figure 2.14 A graph to show expected and actual resonant frequencies that needs to be applied to focus the particles in the main channel.

This phenomenon of this big variance compared to the other steps can be seen in the graph shown in **Fig. 2.15**. This could be one of the reasons of overheating since it required 800 mV as being the biggest voltage required to run the PZT.

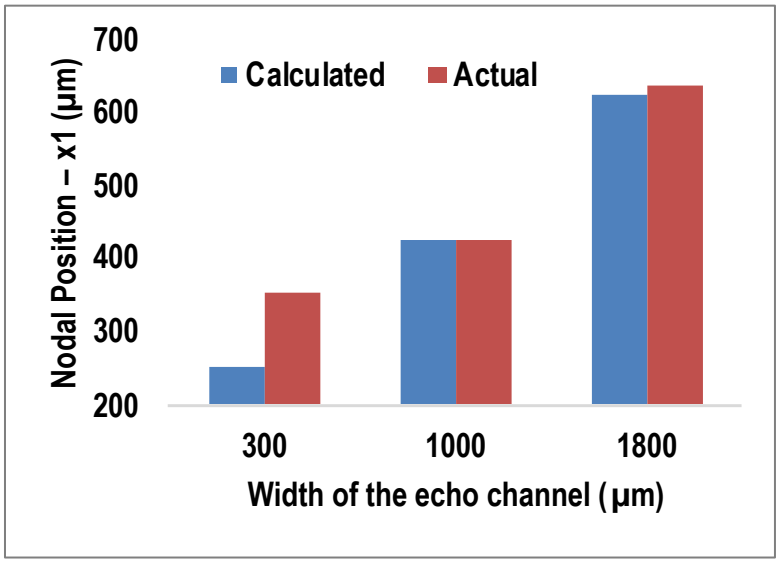

Figure 2.15 A graph showing expected and actual nodal positions.

The minimum required voltages to be able to focus the microparticles at certain acoustic pressure nodes are provided in **Table 2.3**. When overheating occurs the resonant frequency needs to be tuned again to focus the microparticles successfully. To avoid overheating of the acoustofluidic chip frequencies requiring high voltage to overcome the impedance of the piezoelectric transducer can be eliminated. Therefore, requirement of high power can be diminished, and overheating issue of acoustofluidic platforms can be solved by choosing the appropriate piezoelectric transducer.

2.4. Conclusion

Acoustofluidics has been preferred as opposed to the other methods in microfluidics since it makes label-free, contactless and high-throughput manipulation possible. However, nodal positions' being fixed at certain locations restricts its abundant usage. To overcome this issue, fluidic boundary was decoupled from the acoustic

boundary by adding a second bypass channel that is adjacent to the main channel so that acoustic pressure nodes in the upper stream could be moved to the second channel by running the PZTs in second harmonic mode. Therefore, the position of the nodes was successfully adjusted by tuning the resonant frequency after designing the acoustofluidic chips with appropriate channel dimensions.

In the present study, it was observed that the impedance of the piezoelectric transducer has an effect on actuation since the voltage required to overcome the electrical impedance of the transducer is strictly dependent on the frequency. First set of devices the main channel width was chosen as 1600 μm. However, this made frequency range narrow through different echo-channel widths. Because of that, second set of devices channel dimensions are reduced so that frequency range to be tuned to focus the microparticles was broadened. It is important to note that while actuating the acoustic microfluidic chips frequency selection needs to be considered so that overheating of acoustic microfluidic chips can be decreased by reducing the electrical impedance. As a summary, the idea of adding echo-channel next to the main fluidic channel was implemented and it was tried to optimize addressed how the problem of fixed-nodal position can be decreased by designing the channel geometries with appropriate parameters. Finally, a staircase echo-channel was designed, and this chip provided better capability in terms of changing the positions of acoustic pressure nodal positions inside the main fluidic channel.

References

1. Antfolk, M., Magnusson, C., Augustsson, P., Lilja, H., & Laurell, T. (2015). Acoustofluidic, label-free separation and simultaneous concentration of rare tumor cells from white blood cells. Analytical chemistry, 87(18), 9322-9328.

2. Lenshof, A., Magnusson, C., & Laurell, T. (2012). Acoustofluidics 8: Applications of acoustophoresis in continuous flow microsystems. Lab on a Chip, 12(7), 1210-1223.

3. Wang, H., Liu, Z., Kim, S., Koo, C., Cho, Y., Jang, D. Y., ... & Han, A. (2014). Microfluidic acoustophoretic force based low-concentration oil separation and detection from the environment. Lab on a Chip, 14(5), 947-956.\

4. Ding, Xiaoyun, Sz-Chin Steven Lin, Brian Kiraly, Hongjun Yue, Sixing Li, I-Kao Chiang, Jinjie Shi, Stephen J. Benkovic, and Tony Jun Huang. "On-chip manipulation of single microparticles, cells, and organisms using surface acoustic waves." Proceedings of the National Academy of Sciences109, no. 28 (2012): 11105-11109.

5. Wang, H., Liu, Z., Shin, D. M., Chen, Z. G., Cho, Y., Kim, Y. J., & Han, A. (2018). Single-cell compressibility quantification for assessing metastatic potential of cancer cells through multi-frequency acoustophoresis. Microfluidics and Nanofluidics, 22(6), 68.

6. Wiklund, M., Christakou, A., Ohlin, M., Iranmanesh, I., Frisk, T., Vanherberghen, B., & Önfelt, B. (2014). Ultrasound-induced cell–cell interaction studies in a multi-well microplate. Micromachines, 5(1), 27-49.

7. Evander, M., & Nilsson, J. (2012). Acoustofluidics 20: Applications in acoustic trapping. Lab on a Chip, 12(22), 4667-4676.

8. Destgeer, G., Cho, H., Ha, B. H., Jung, J. H., Park, J., & Sung, H. J. (2016). Acoustofluidic particle manipulation inside a sessile droplet: four distinct regimes of particle concentration. Lab on a Chip, 16(4), 660-667.

9. Fornell, A., Nilsson, J., Jonsson, L., Periyannan Rajeswari, P. K., Joensson, H. N., & Tenje, M. (2015). Controlled lateral positioning of microparticles inside droplets using acoustophoresis. Analytical chemistry, 87(20), 10521-10526.

10. Wiklund, M., Günther, C., Lemor, R., Jäger, M., Fuhr, G., & Hertz, H. M. (2006). Ultrasonic standing wave manipulation technology integrated into a dielectrophoretic chip. Lab on a Chip, 6(12), 1537-1544.

11. Leibacher, I., Schatzer, S., Dual, J. (2014). Impedance matched channel walls in acoustofluidic systems," Lab on a Chip, Vol. 14, No. 3, pp. 433-610.

12. Jung, S. Y., Notton, T., Fong, E., Shusteff, M., & Weinberger, L. S. (2015). Spatial tuning of acoustofluidic pressure nodes by altering net sonic velocity enables high-throughput, efficient cell sorting. Lab on a Chip, 15(4), 1000-1003.

13. Fong, E. J., Johnston, A. C., Notton, T., Jung, S. Y., Rose, K. A., Weinberger, L. S., & Shusteff, M. (2014). Acoustic focusing with engineered node locations for high-performance microfluidic particle separation. Analyst, 139(5), 1192-1200.

14. Haynes, William M. CRC handbook of chemistry and physics. CRC press, 2014.

15. Cushing, K.W., Garofalo, F., Magnusson, C., Ekblad, L., Bruus, H. and Laurell, T., 2017. Ultrasound characterization of microbead and cell suspensions by speed of sound measurements of neutrally buoyant samples. Analytical chemistry, 89(17), pp.8917-8923.

16. Hopcroft, M.A., Nix, W.D. and Kenny, T.W., 2010. What is the Young's Modulus of Silicon? Journal of microelectromechanical systems, 19(2), pp.229-238.

17. Arnold, F. J., Gonçalves, M. S., Bravo-Roger, L. L., & Mühlen, S. S. (2015). Electric impedance of piezoelectric ceramics under acoustic loads. ECTI Transactions on Electrical Engineering, Electronics, and Communications, 12(2), 48-54.

3. ACOUSTOPHORETIC SEPARATION OF BINARY PARTICLES BASED ON NODAL POSITION ADJUSTMENT THROUGH PDMS WALL

3.1. Introduction

To date to answer different kind of issues come across in the field of microfluidics number of different applications was studied and tried such as hydrodynamic separation [1], dielectrophoresis [2], magnetophoresis [3], microfabricated filtering [4], droplet microfluidics [5] and acoustofluidics [6]. Acoustofluidics has provided high-throughput cell/particle manipulation in a contact-free manner. While some of the researchers in this field worked on cell property analysis [7,8,9] and some of them studied cell/particle separation [10,11], extensively. Even though the advantage of acoustics microfluidics systems is undeniable it has some restrictions because of its dependence on channel dimensions. The particles/cells migrate to certain locations in an acoustofluidic system where acoustic pressure is zero or maximum. In the acoustic wave theory those positions are called as acoustic pressure node (zero pressure) or anti-nodes (maximum pressure). Once the channel is fabricated the nodal planes are fixed at certain positions inside the fluidic channel. However, if the fluidic boundary is shifted from the acoustic boundary by the help of appropriate material those locations inside the fluidic channel can be shifted relatively. In 2015 paper, Jung et al. showed the possibility of separation of acoustic boundary from the fluidic boundary by fabricating a thin silicon wall between main channel and so-called by-pass channel [12]. They showed the possibility of changing the acoustic nodal positions inside the main channel by varying the fluid inside the by-pass

channel. However, it required the thin wall thickness to be less than 20 μm to generate a successful acoustic resonance during the implementation. Similarly, Ivo et al. fabricated a PDMS wall by laser cutting in an acoustofluidic chip so that fluidic boundary was decoupled from one of the silicon walls (acoustic boundary) [13]. They demonstrated particle and droplet manipulation by using so-called partially filled PDMS acoustic microfluidic chip. In **Fig. 3.1**, the effect of PDMS wall integration into the acoustic pressure nodes can be seen. Since the speed of sound inside the PDMS is slower than in the water the acoustic wave will travel slower in the PDMS region. Because of that reason the acoustic pressure nodal positions will move towards the PDMS wall side. Even though implementing integration of the PDMS wall into acoustofluidic chip by laser cutting is promising that method require a costly and precise equipment such as laser to make the PDMS layer since after filling the channel one part of the PDMS structure needs to be cut by laser. On the other hand, it is difficult to fabricate the desired size of PDMS because of the laser spot size. Another limitation is operation of laser could be challenging since safety precautions need to be taken. In this study, we summarized an easier fabrication method to integrate PDMS wall into the side of the microfluidic channel when compared to laser cutting. First, we etched the silicon channel using wet etching process by adding some amount of isopropyl alcohol so that aspect ratio of etch profile was increased [14]. PDMS microparticles were emulsified in DI water and synthesized by following the recipe in Cushing et. al. [15]. Following the fabrication of silicon mold using photolithography and by employing soft lithography techniques PDMS wall was cured in this mold and could be used as a side wall inside the microfluidic channel so that decoupling of fluidic

boundary from the acoustic boundary was successfully implemented. In this research we addressed how we can eliminate the requirement of high-cost equipment such as laser and use cost-effective photolithographic methods to integrate the PDMS wall into the acoustic microfluidic chip.

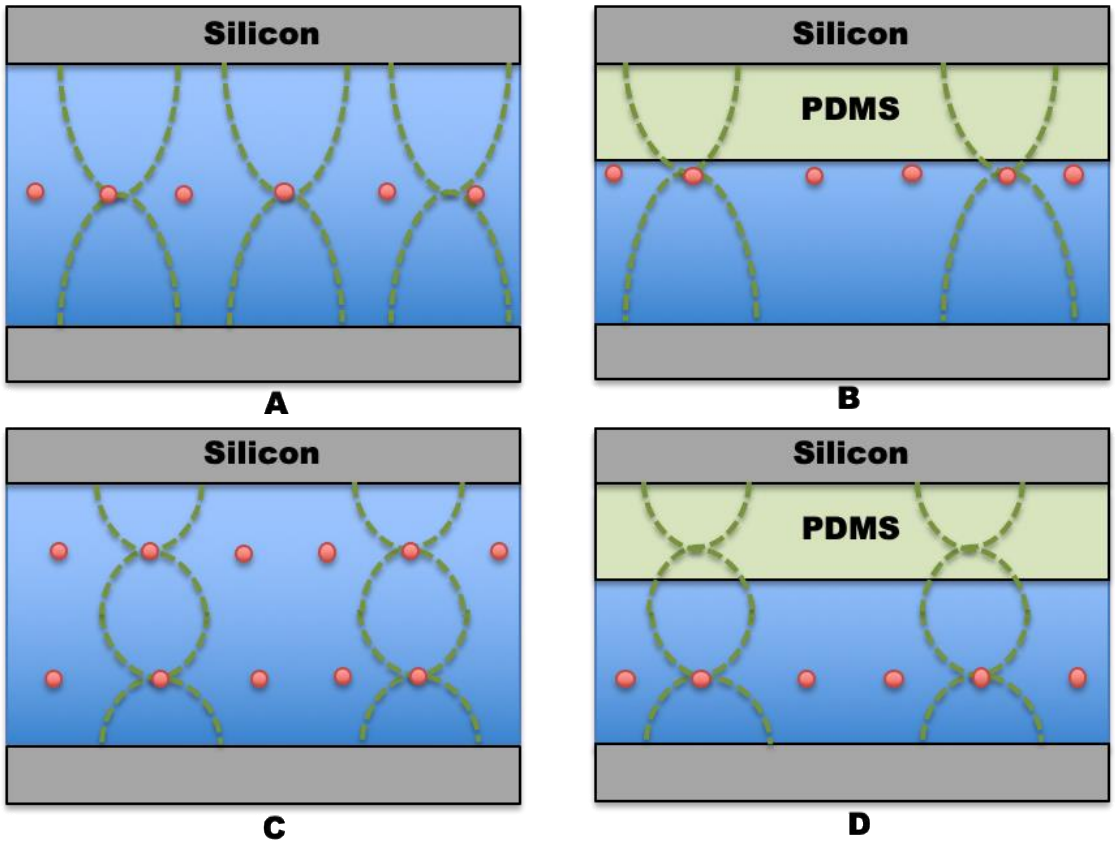

Figure 3.1 Acoustic pressure nodal positions in microfluidic channel in a conventional BAW device when PZT is actuated using first harmonic (**λ**/2) mode **(A)**, Nodal positions in microfluidic channel in partially-filled PDMS acoustic chip using first harmonic (**λ**/2) mode **(B)**, Nodal positions in microfluidic channel in a conventional BAW device using second harmonic (**λ**) mode **(C)**, Nodal positions in microfluidic channel in partially-filled PDMS acoustic chip using second harmonic (**λ**) mode **(D)**.

3.2. Materials and Methods

PDMS is a very popular material in microfluidics since it is easy to fabricate by just mixing two different solution at certain ratio. Because of being transparent, flexible, biocompatible, PDMS is preferred for microfluidic applications since those applications require microscope imaging of biological cells, reagents, etc. It is not preferred for acoustofluidic projects because of PDMS having lower acoustic impedance when compared to silicon and glass substrates. However, reducing the PDMS thickness enough may eliminate this disadvantage. To fabricate the acoustic microfluidic chip first, silicon wafers were oxidized using the oxidation furnace (MiniBrute Atmospheric Furnace, Thermco, NJ, USA) and thickness of 1 μm was achieved. Silicon wafer was etched using standard wet etching process after transferring the pattern for channel and mold designs. For wet etching process 40 weight % potassium hydroxide (KOH) solution (solid dissolved in water) was prepared by mixing KOH pellets (ThermoFisher Sci, MA, USA) with deionized (DI) water. After etching the wafers for nearly 60 μm deep, the wafers were diced into four pieces. Then, they were classified into two categories. The ones with small widths are used for PDMS fabrication and were treated with silane (Trichloro(1H,1H,2H,2H-perfluorooctyl)silane, Millipore Sigma, MO, USA). The wider ones are used as microfluidic channel. To fabricate the PDMS wall, the mixture was prepared by mixing the curing agent and the base material for PDMS (Sylgard 184, USA). Then they are poured into a weigh boat at a ratio of 1:10 and mixed vigorously. After this mixing process it was poured into the silane-coated silicon mold and degassed inside the

degassing chamber. To fabricate PDMS wall to have a thickness of less than 60 µm needs the mold was spun at 1000 rpm for 40 seconds. After spinning the molds were left in 85°C oven for 8 hours so that it can be easily peeled off from the silicon mold. Since low acoustic impedance of PDMS might absorb most of the acoustic energy it is better to make the PDMS wall as thin as possible. Therefore, it won't require too much voltage during the excitation of acoustofluidic chip.

Following the fabrication of the PDMS wall the holes were punched using a 500 µm punch and it was bonded to the silicon channel using the oxygen plasma chamber (Harrick Plasma, USA) so that silicon and PDMS can be successfully sealed to avoid any leakages during the experiments. The fluidic access holes were drilled on the borosilicate glass (Swift Glass, NY, USA) using a platinum coated drill bit (UKAM Industrial Superhard Tools, CA, USA) and a benchtop drill press (DP101, Ryobi Ltd, SC, USA). Then, glass cover was bonded to the PDMS layer after the plasma treatment process of both surfaces. Fabrication processes are summarized in **Fig. 3.2A-D**.

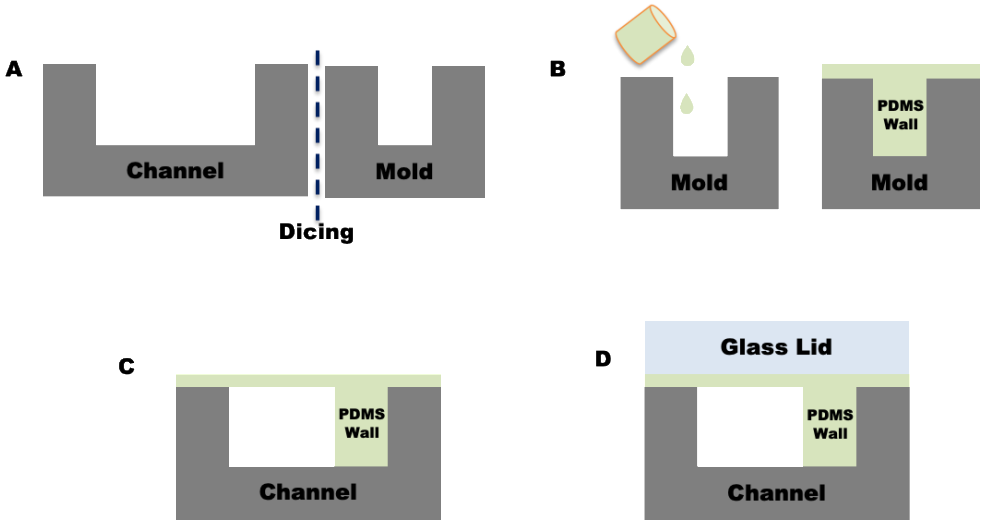

Figure 3.2 Fabrication steps to integrate PDMS wall into acoustofluidic platform **(A-D)**.

After the bonding process ferrules (P-200N, IDEX-HS, WA, USA) were glued onto the glass surface using epoxy (Gorilla, USA). The tubings (Tygon, Saint Gobain Performance Plastics, OH, USA) were inserted into those ferrules and sealed with epoxy. Once epoxy mixture is cured the piezoelectric transducer (PZ26, Ferroperm, Denmark) was attached on the bottom surface of silicon substrate using cyanoacrylic glue (Loctite, USA). The wires to actuate the PZT were soldered onto the bottom and top surface of the PZT. Scanning electron microscopy (SEM) image of the fabricated acoustofluidic chip can be seen in **Fig. 3.3**.

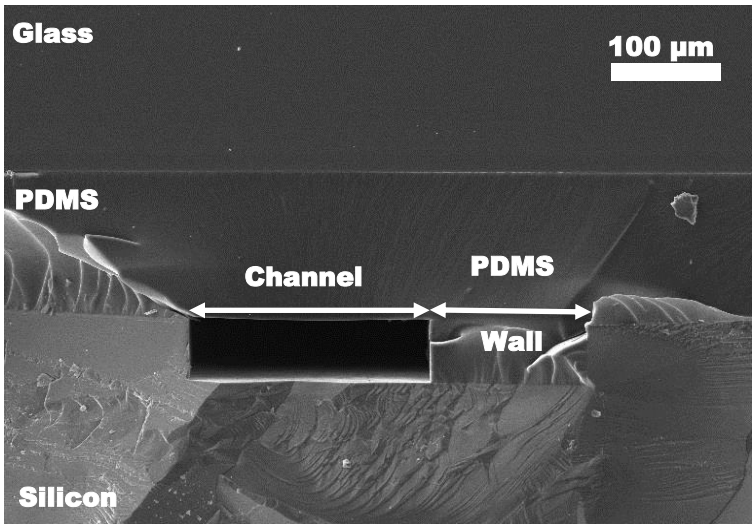

Figure 3.3 SEM image of the fabricated acoustofluidic chip with PDMS wall.

Acoustofluidic device illustration for separating the negative and positive acoustic contrast particles by the help of acoustophoresis is shown in **Fig. 3.4**. As seen from this figure polystyrene microspheres will migrate to acoustic pressure nodes and PDMS microspheres will migrate to acoustic pressure anti-nodes.

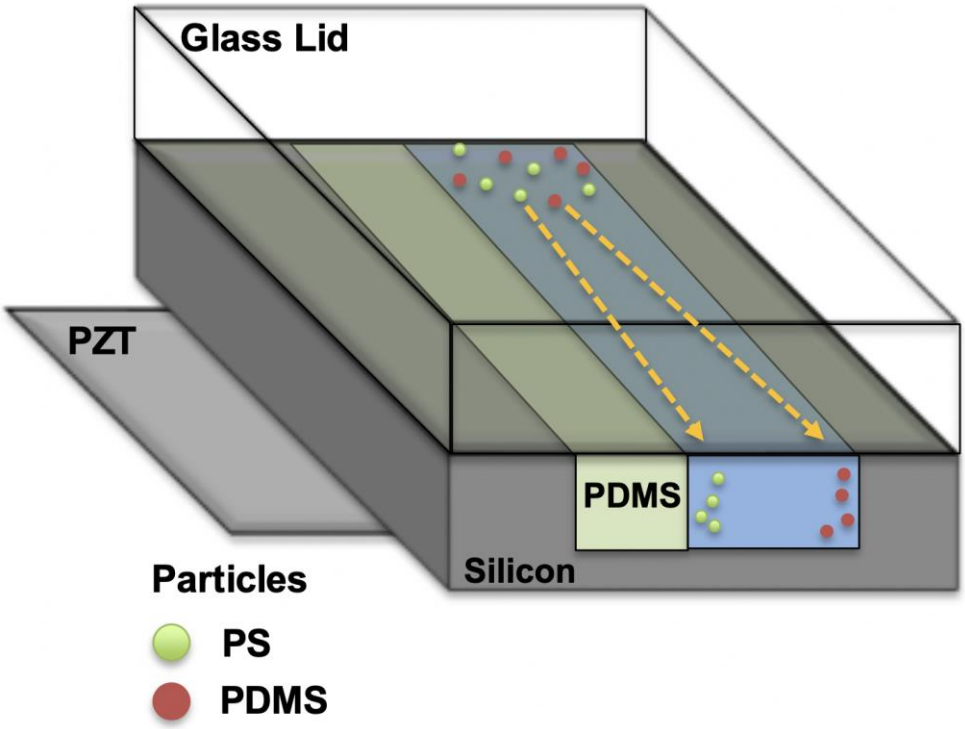

Figure 3.4 Illustration of negative (PDMS) and positive (Polystyrene) acoustic contrast particle migration inside acoustic microfluidic chip.

3.3. Results

3.3.1. Simulation Results Using Finite Element Analysis (FEA)

Acoustic pressure nodes were analyzed by simulating the acoustofluidic chip with finite element analysis software before running the experiments with the chip. For that reason, 2-D model was created in COMSOL Multiphysics software (**Fig. 3.5A**) and appropriate materials were assigned to the model structures. PDMS was assigned to the upper rectangle and water was assigned to the lower rectangle as materials. For analysis smaller elements of 2-D model was generated using the `finer` mesh function in the

software as seen in **Fig. 3.5B**. In this model fluidic channel width is 225 μm and width of the PDMS wall is 150 μm.

Figure 3.5 A. 2-D model in COMSOL when fluidic channel width is 225 μm (lower part of the rectangle) and width of the PDMS wall (upper part of the rectangle) is 150 μm B. Model after using the mesh function in COMSOL model.

Applying frequency of 1.70 MHz yielded result of shift the acoustic pressure nodes from the middle to closer to the PDMS wall. Simulation result after applying the resonant frequency is shown in **Fig. 3.6**. As seen from the figure, acoustic pressure nodal line (dark blue line) moves closer to the PDMS wall in contrast to being in the middle when there is no PDMS slab in the microfluidic channel.

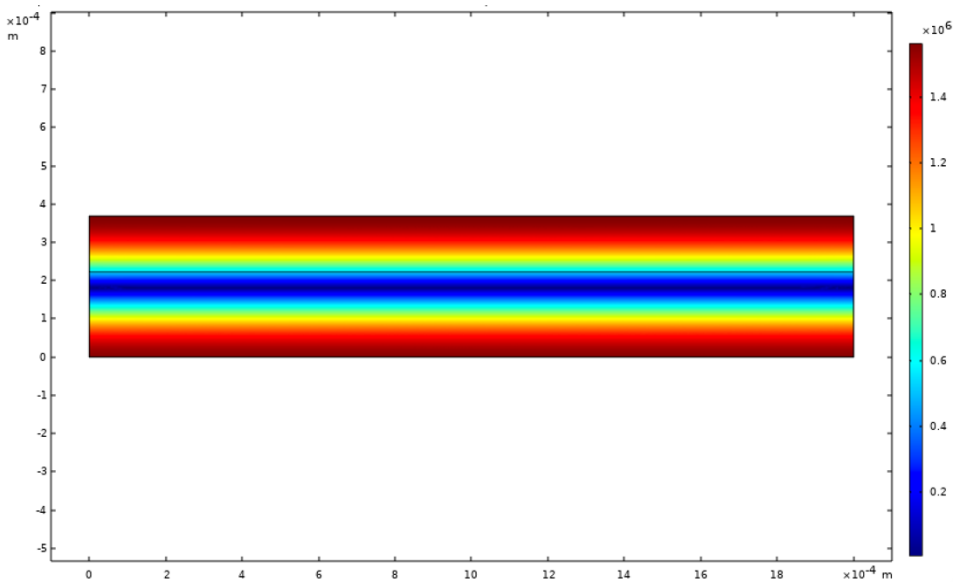

Figure 3.6 Plot of acoustic pressure inside the microchannel when applied frequency is 1.70 MHz.

3.3.2. Experimental Results

Before running the experiments. Sinusoidal wave was generated using a waveform generator (AFG3021B, Tektronix, OR, USA) and amplified through a 50-dB power amplifier (2100L, E&I, NY, USA) before reaching the ends of PZT. Once 10 µm polystyrene (PS) microbeads (Polysciences, PA, USA) were flown the PZT is actuated and resonant frequency was tuned for half wavelength resonance mode (f_0). The resonant frequency to move the PS microbeads toward the acoustic pressure node was 2.58 MHz and the applied peak-peak voltage at the ends of amplifier was 200 mV. Similarly, synthesized PDMS microparticles were flown through the microfluidic channel. Since they behave as negative acoustic contrast particles, they migrate to the acoustic pressure anti-node at the same applied frequency and voltage. If there was no PDMS wall inside

the microfluidic channel the expected resonant frequency for the acoustofluidic chip would be 2 MHz since the silicon channel width is 375 µm. However, adding a PDMS wall will decrease the speed of sound in that region. Because of that the resonant frequency needs be less than 2 MHz. If whole channel was covered with PDMS the resonant frequency would be 1.36 MHz since speed of sound in PDMS is ~1019 m/s [14]. Expected resonant frequency is 1.69 MHz in half wavelength mode and real resonant frequency is 1.75 MHz. In **Fig. 3.7A&B** microscopic images of PS particle migration to acoustic pressure nodes and PDMS particle moving to anti-nodes can be seen.

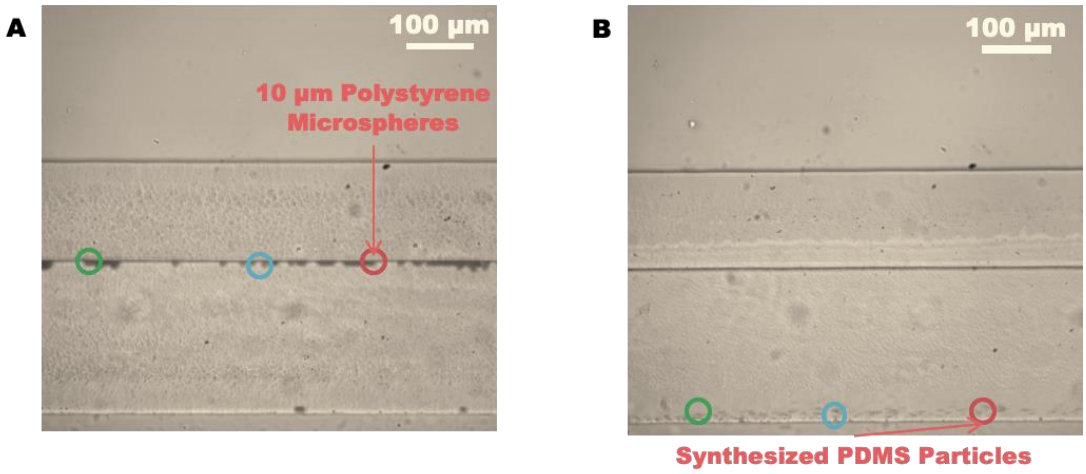

Figure 3.7 BF microscopic images (Exposure time: 10 ms) to show 10 µm polystyrene moving randomly **(A)** to show 10 µm polystyrene microbeads migration towards the acoustic pressure nodes when f=1.75 MHz and Vpp=200mV **(B)**.

The width of the PDMS wall was reduced from ~145 µm to ~125 µm in another acoustofluidic platform. To focus the polystyrene microspheres to the center in this case PZT was run at 2.88 MHz and the applied peak-peak voltage was 150 mV. As seen in **Fig. 3.8A** 15 µm polystyrene microspheres migrate to ~150 µm apart from the lower silicon

wall. This shows that effective channel width of the acoustofluidic platform was increased by adding a PDMS wall. When the applied frequency was changed to 1.44 MHz and the peak-peak voltage was increased to 200 mV the microbeads just migrated towards the PDMS slab since effective channel width is much wider than width of the silicon channel. (**Fig. 3.8B**)

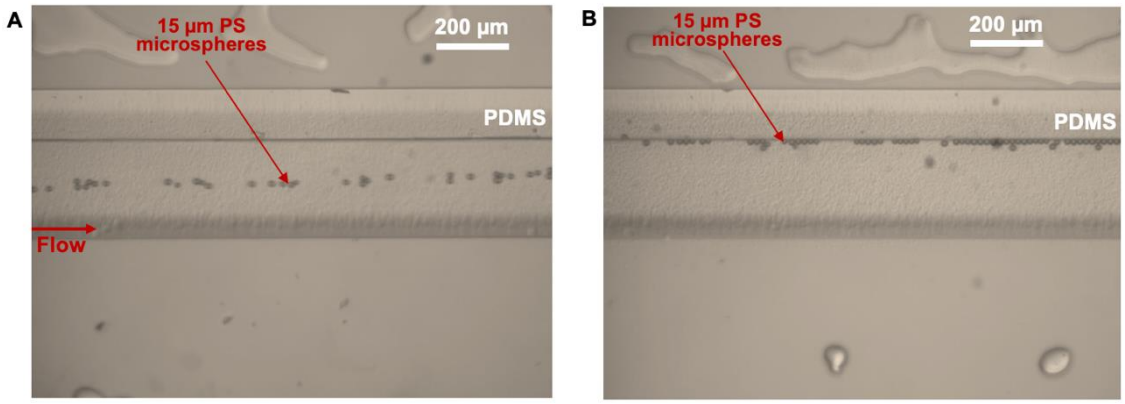

Figure 3.8 A. Migration of 15 µm PS microspheres to acoustic pressure nodal position when PZT is run at 2.88 MHz and 150 mV_{pp} **B.** Levitation of PS microspheres when acoustofluidic chip is run at fundamental (**λ**/2) mode.

The method of integrating the PDMS wall is easy since it doesn't require any high-technology equipment and can be fabricated using soft lithography methods. Also this cost-efficient method can be exploited to guide particles/cells in an acoustic microfluidic chip so that particles can follow the desired flow manner.

3.4. Conclusion

Being contactless, label-free and high-throughput makes acoustofluidics preferable as opposed to the other methods in microfluidics. Though it provides effective

microfluidic manipulation its common usage is limited because of fixed acoustic pressure nodal positions. To overcome this issue, fluidic boundary was decoupled from the acoustic boundary by integrating a PDMS wall into acoustofluidic device so that the position of the nodes was successfully adjusted by tuning the resonant frequency to generate acoustic resonance in different harmonic modes.

In the present study, the developed acoustofluidic chip is based on the concept of decoupling the acoustic boundary from the fluidic boundary by using cost-effective fabrication. For that reason, PDMS wall was successfully integrated into the microfluidic channel by the help of soft lithography techniques. This method let us successfully separate negative acoustic contrast particles from positive acoustic contrast particles. Integration of PDMS structure into acoustic microfluidic channel can be exploited so that conventional microfluidic techniques can be used to take advantage of label-free, contactless manipulation of cells/particles in acoustofluidics.

References

1. Huh, Dongeun, et al. "Gravity-driven microfluidic particle sorting device with hydrodynamic separation amplification." Analytical chemistry 79.4 (2007): 1369-1376.
2. Gascoyne PR, Vykoukal J. Particle separation by dielectrophoresis. Electrophoresis. 2002 Jul;23(13):1973-83.
3. Zborowski M, Ostera GR, Moore LR, Milliron S, Chalmers JJ, Schechter AN. Red blood cell magnetophoresis. Biophysical journal. 2003 Apr 1;84(4):2638-45.
4. He B, Tan L, Regnier F. Microfabricated filters for microfluidic analytical systems. Analytical Chemistry. 1999 Apr 1;71(7):1464-8.
5. Laurell T, Petersson F, Nilsson A. Chip integrated strategies for acoustic separation and manipulation of cells and particles. Chemical Society Reviews. 2007;36(3):492-506.
6. Kim HS, Guzman AR, Thapa HR, Devarenne TP, Han A. A droplet microfluidics platform for rapid microalgal growth and oil production analysis. Biotechnology and bioengineering. 2016 Aug;113(8):1691-701.
7. Augustsson P, Karlsen JT, Su HW, Bruus H, Voldman J. Iso-acoustic focusing of cells for size-insensitive acousto-mechanical phenotyping. Nature communications. 2016 May 16;7:11556.
8. Li S, Guo F, Chen Y, Ding X, Li P, Wang L, Cameron CE, Huang TJ. Standing surface acoustic wave based cell coculture. Analytical chemistry.2014 Sep 18;86(19):9853-9.

9. Wang H, Liu Z, Shin DM, Chen ZG, Cho Y, Kim YJ, Han A. A continuous-flow acoustofluidic cytometer for single-cell mechanotyping. Lab on a Chip. 2019;19(3):387-93.
10. Destgeer G, Im S, Hang Ha B, Ho Jung J, Ahmad Ansari M, Jin Sung H. Adjustable, rapidly switching microfluidic gradient generation using focused travelling surface acoustic waves. Applied Physics Letters. 2014 Jan 13;104(2):023506.
11. Destgeer G, Lee KH, Jung JH, Alazzam A, Sung HJ. Continuous separation of particles in a PDMS microfluidic channel via travelling surface acoustic waves (TSAW). Lab on a Chip. 2013;13(21):4210-6.
12. Jung SY, Notton T, Fong E, Shusteff M, Weinberger LS. Spatial tuning of acoustofluidic pressure nodes by altering net sonic velocity enables high-throughput, efficient cell sorting. Lab on a Chip. 2015;15(4):1000-3.
13. Leibacher I, Schatzer S, Dual J. Impedance matched channel walls in acoustofluidic systems. Lab on a Chip. 2014;14(3):463-70.
14. Monteiro T, Kastytis P, Gonçalves L, Minas G, Cardoso S. Dynamic wet etching of silicon through isopropanol alcohol evaporation. Micromachines. 2015 Oct;6(10):1534-1545.
15. Cushing KW, Piyasena ME, Carroll NJ, Maestas GC, López BA, Edwards BS, Graves SW, López GP. Elastomeric negative acoustic contrast particles for affinity capture assays. Analytical chemistry. 2013 Feb 5;85(4):2208-2215.

4. ACOUSTOFLUIDIC CHIP WITH INTEGRATED MICROVALVES

4.1. Introduction

As discussed in the previous chapters combining acoustics with microfluidics technology let successful demonstration of different microfluidic applications in a label-free and contactless manner. To name a few in the literature culture medium exchange, cell purification, cell/particle separation and plasmapheresis can be summarized [1,2,3,4]. As mentioned in introduction section layered resonators and surface acoustic wave (SAW) devices are other two configurations that enable acoustofluidic microsystems. Spengler *et al.* have demonstrated the construction of a layered resonator in microfluidic systems using spacer transducer between the counting chamber and glass reflector to measure the yeast cell concentration [5]. However, in that study it was needed to do a precise alignment to let resonance occur. Otherwise, some of the cells cannot be driven into the pressure nodal planes and will be dragged by the stream. In SAW devices, pairs of interdigitated electrodes (IDTs) patterned on piezoelectric materials create travelling or standing SAW (TSAW or SSAW) inside microchannels [6]. They used PDMS as a substrate to fabricate the microfluidic channel and PDMS was placed on top of the patterned IDTs so that more flexible fluid manipulation can be succeeded. However, since IDTs are closely located to the PDMS microchannel those devices may suffer from heat generation. SAW devices require acoustic streaming at high actuation frequencies. Besides that, piezoelectric materials used for SAW devices such as lithium niobate ($LiNbO_3$) can be relatively costly when compared to the materials used in bulk acoustic wave (BAW) based systems. BAW

devices are preferred by many researchers because of strong primary radiation forces and having cost-effective fabrication [7,8]. Though easy to fabricate and use, these transversal resonator-type acoustofluidic systems usually have very limited material choices, mainly silicon and glass, greatly limiting the possibilities where such acoustic-based microfluidic systems can be utilized. This is due to the fact that hard materials such as silicon and glass transmit acoustic wave with limited loss, while soft polymer materials such as the commonly used polydimethyl siloxane (PDMS) have large acoustic loss, and thus does not support an acoustic standing wave. Although cell manipulation (both separation and trapping) is possible using acoustophoresis, fluid manipulation such as stopping the flow or switching liquid are not possible using acoustophoresis. Integrating microvalves can solve this issue, however doing so in a silicon or glass microfluidic channel is quite challenging.

Contrary to this, in PDMS-based microfluidic systems integrating pneumatically actuated microvalves into microfluidic channels is relatively easy. PDMS is used as the basic material for many microfluidic applications due to its advantages of being biocompatibility, transparency, elasticity, and ease of fabrication [9]. These traits enable observation and manipulation of particles and cells as well as fluids inside a microchannel. Therefore, it is of great interest to integrate PDMS in acoustic microsystems to enable more flexible particle/cell manipulation, as well as fluid manipulation, while also enabling cell culture. Since PDMS was used extensively in microfluidic devices because of ease of fabrication PDMS membrane was used to actuate microvalves in some applications of microfluidics [10,11]. An acoustofluidic lab-on-a-chip system that integrates PDMS-

based microfluidic valves and membranes into silicon/glass microfluidic channels to enable better fluidic control can greatly expand the applications where acoustofluidic systems can be utilized. However, due to its low acoustic impedance PDMS itself cannot act as an acoustic reflector and thus its use has been limited in acoustofluidic microsystems. Leibacher *et al.* showed that by applying PDMS inside a microchannel where acoustic standing wave will be generated, the pressure nodes and antinodes can be adjusted according to the PDMS structure and the acoustic boundary can be separated from the fluidic boundary [12]. This shows the possibility that acoustic microsystems can benefit from proper integration with PDMS as structural material in BAW devices.

Here we present for the first time, the construction of a silicon/glass acoustofluidic microsystem that integrates a PDMS membrane to enable cell culture as well as integrates pneumatically actuated PDMS microvalves to enable fluid control, while also allowing cell manipulation using bulk acoustic wave. As illustrated in **Fig. 4.1** PDMS membrane will be functioning as a structural material to actuate the microvalve because its elasticity.

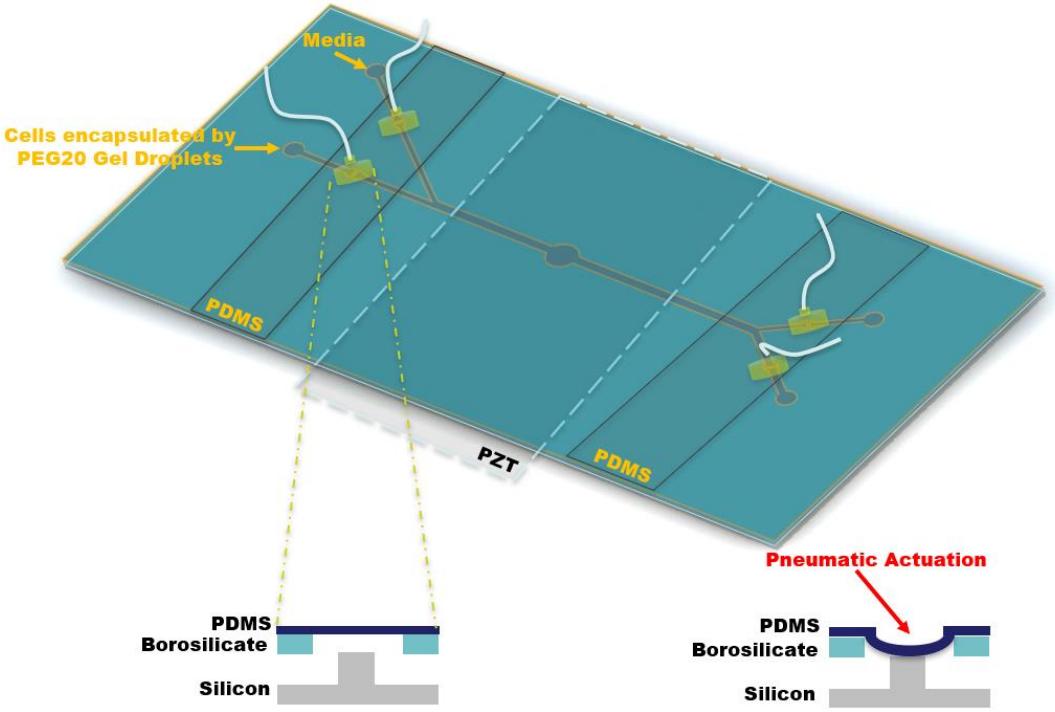

Figure 4.1 Illustration of acoustofluidic trapping chip with integrated microvalves.

The valve structure was designed to be a normally open valve and once the PDMS membrane is bended because of pneumatic actuation it will stop the flow inside the microchannel. This acoustofluidic platform let us manipulate hydrogel droplets inside a trapping chamber and change the medium which surrounds them. These gel droplets let researchers keep the cells in three dimensional (3D) scaffolds. This can be the first step towards a complete acoustofluidic lab-on-a-chip system for more versatile biological and biomedical applications using bulk acoustic wave.

Before designing the acoustofluidic platform with integrated microvalves we first assessed the information of particle trapping efficiency of different trapping chambers.

For that reason, acoustofluidic device consisting of circles with three different diameters was designed and fabricated. Illustration of this device is shown in **Fig. 4.2** and fabrication steps of these two acoustofluidic platforms are summarized in the following section.

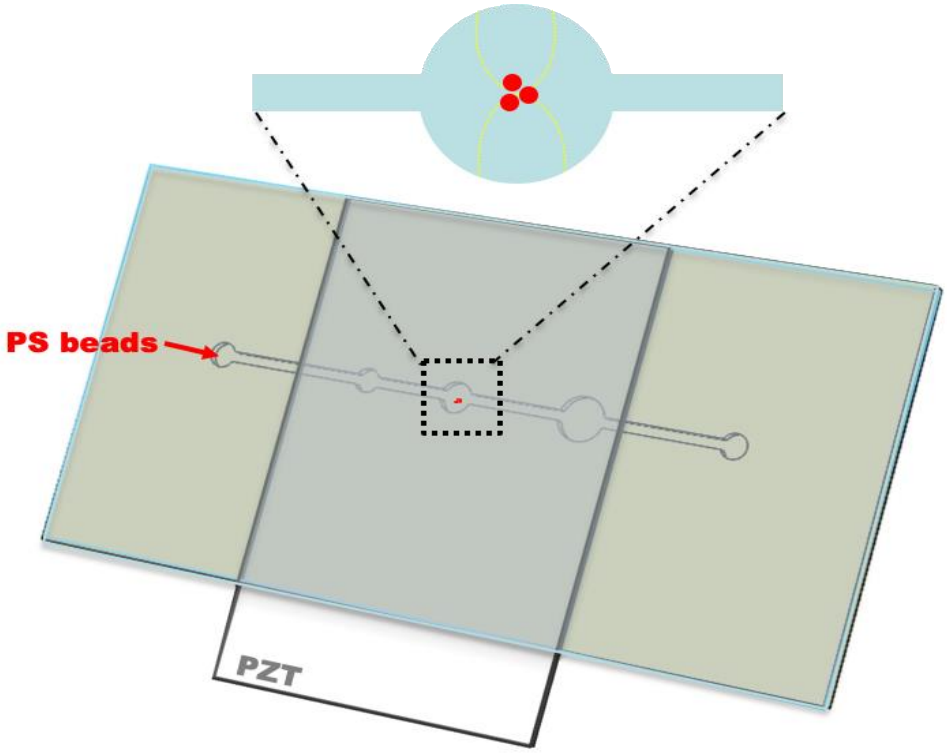

Figure 4.2 Illustration of acoustofluidic device consisting trapping chambers with different diameters.

The purpose of this platform to trap the polystyrene microbeads into the center of the circular chamber and find the minimum required voltage to keep the particles at the same position when flow is continuous.

4.2. Materials and Methods

Acoustofluidic device to characterize the trapping capability of different chamber was fabricated by using the following steps. First, the microfluidic channel designs were patterned by photolithography on a silicon wafer and then etched into the silicon substrates using deep reactive ion etching (DRIE) to a depth of 105 μm. Fluidic access holes were drilled in a borosilicate glass substrate using a diamond-plated drill bit mounted on a benchtop drill press (DP101, Ryobi Ltd, SC, USA). The glass and silicon layer were anodically bonded at 420 °C by applying 710 V of DC voltage for one hour. Following the bonding process, ferrules (P200-N, IDEX Health & Science, WA, USA) were glued onto the holes of the glass layer using epoxy for fluidic access. Flexible polymer tubings (Tygon, Saint Gobain Performance Plastics, OH, USA) were inserted inside the ferrules and sealed with epoxy (Gorilla Glue, OH, USA). The PZ26 type PZT (Ferroperm, Denmark) was bonded to the bottom of the chip with cyanoacrylic glue (Loctite, USA), and wires were soldered to the PZT for electrical interconnect.

For the second acoustofluidic device to integrate microvalves was fabricated by following the steps in the above paragraph and these steps. While the holes for fluidic access were drilled in the glass the holes for pneumatic access were also drilled. At this moment the holes need to be properly aligned so that microvalves can be operated successfully. PDMS membrane to actuate microvalve structures were fabricated by mixing the PDMS (DOW Sylgard 184, MI, USA) and pouring into a transparent film (Apollo CG7060, Acco Corp, IL, USA) attached onto poly-methyl methacrylate (PMMA) and spun at 3000 route per minute (rpm) for 40 seconds yielded 30 μm of thickness.

Fabricated PDMS membrane was bonded to the glass substrate by using plasma (Harrick Plasma, NY, USA) treatment. After that same ferrules were attached on top of the microvalve beds and sealed with epoxy following the tubing insertion. Fabrication steps are summarized in **Fig. 4.3**.

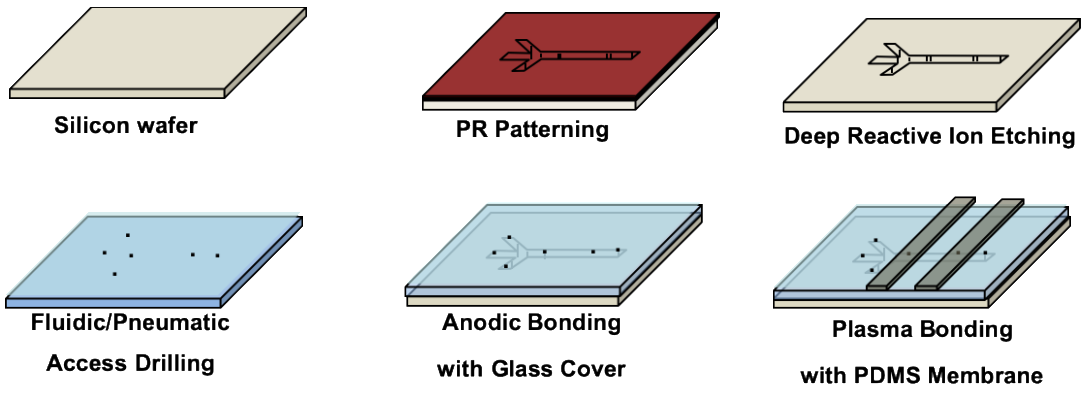

Figure 4.3 Fabrication steps for acoustofluidic chip with integrated microvalves.

4.3. Results

Acoustofluidic device testing was conducted under an upright microscope (Eclipse LV100D, Nikon Inc, Japan) and fluids were flown through the microchannels by a 4-barrel syringe pump (Fusion 400, Chemyx Inc, MA, USA). The flow rate was chosen to be 50 µL/h. Fluorescent polystyrene microspheres (Thermoscientific, CA, USA) mixed with de-ionized (DI) water was used for characterization of acoustofluidic chips for easy visualization of particle movement. For devices with the straight echo-channel design (single width throughout the length of the microchannel), a function generator (AFG3021B, Tektronix Inc, OR, USA) was utilized to generate a sinusoidal signal that

was amplified through a 50-dB power amplifier (2100L, E&I, Ltd.) and applied to the PZT.

4.3.1. Particle Focusing and Trapping by Acoustophoresis

First assessment was implemented using the straight microfluidic channel which has a width of ~400 μm. In this experiment the channel was filled with fluorescent microparticles which have a diameter of ~10 μm. The expected resonant frequency in this experimental run was ~1.87 MHz and actual resonant frequency after experimental characterization was 1.98 MHz. The microscopic images of before and after acoustic focusing are shown in **Fig. 4.4**.

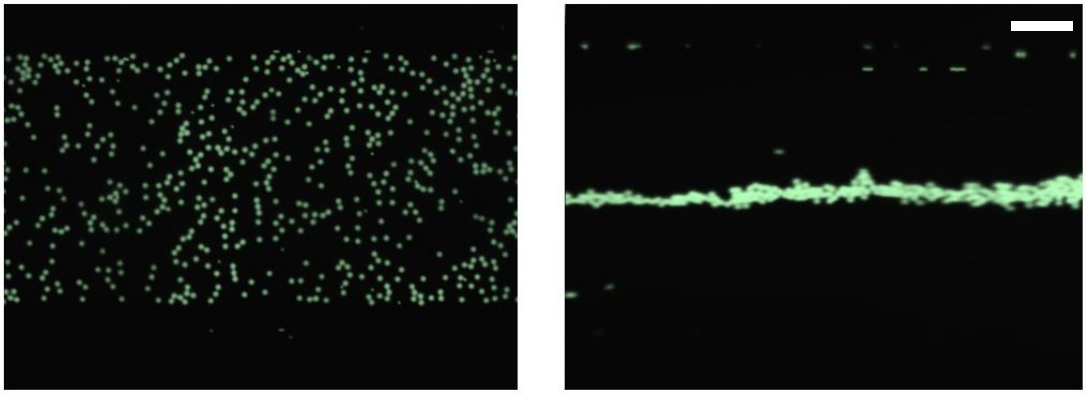

Figure 4.4 Green fluorescent microscopic images to show microparticles (diameter: 12 μm) focused at middle of the straight channel when there is no flow. Resonant frequency of acoustic wave is 1.98 MHz and peak-peak voltage at the ends of power amplifier is 300 mV. (Scale bar is 100 μm.).

Following that 40 μm microspheres are tried to be trapped inside circular chambers while flow rate is kept at 50 μL/h. The diameters of these circular chambers are 500, 750,

and 1200 μm, respectively. For each chamber expected and actual resonant frequencies are summarized in **Table 4.1**.

Table 4.1 Table to show experimental conditions for different size of trapping chambers

Diameter of the chamber (μm)	***Calculated f_0 (MHz)***	***Real f_0 (MHz)***	***Minimum V_{pp} (mV)***	***Forward Power (P_f)***	***Reflected Power (P_r)***
500	1.52	1.58	500	28	25
750	1.02	1.05	180	11	10
1200	0.602	0.65	600	33	27

As seen from the table 750 μm-wide chamber required the minimum voltage to trap the polystyrene microbeads in the center of the chamber. Therefore, 750 μm wide trapping chamber was selected to be used in the acoustofluidic platform with integrated microvalves.

As shown in **Fig. 4.5** PS microbeads were trapped at the center of the chamber. PS microbeads with a diameter of 40 μm to find the minimum power required to trap the micro spherical structures by the help of acoustophoresis in the center of the chamber.

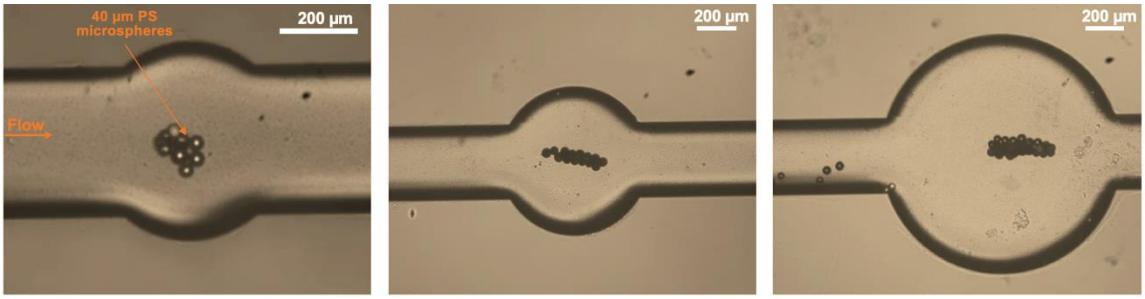

Figure 4.5 Brightfield microscopic images (exposure time: 10 ms) to show microparticle trapping when diameters of the chambers 500 µm (left), 750 µm (middle), 1200 µm (right) from left to right. (Polystyrene microbead diameter is 40 µm).

Following the design and fabrication of acoustofluidic platform hydrogel droplets are generated using a flow focusing droplet generator. Hydrogel droplets are used as three-dimensional (3D) scaffolds for cell culture and functions that cell can grow inside because of its porous structure [13].

4.3.2. Hydrogel Droplet Generation

To generate droplets, flow-focusing based droplet generator was fabricated on a PDMS/Glass microfluidic chip. The widths of the inlets for the hydrogel solution and oil are 80 µm and the depth of the microchannel is 67 µm. Flow rate for gel solution mixed with salmonellae (following the one day of culture it was diluted 20 times to reduce the number of bacteria per droplet) was selected to be 100 µL/h and oil (Novec-7500 Engineering Fluid, 3M Corp, MN, USA) flow rate was selected to be 300 µL/h. As shown in **Fig. 4.6A** generated agarose hydrogel droplets are leaving the flow focusing region of the droplet generator after generation.

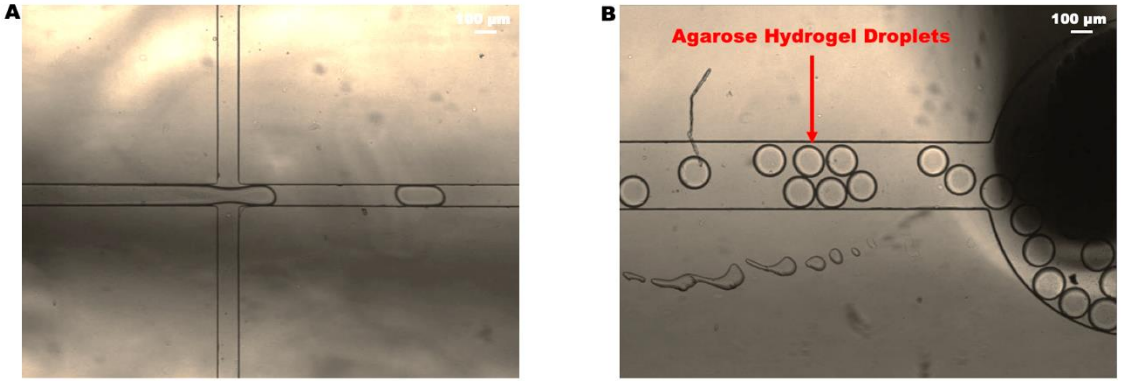

Figure 4.6 A. Encapsulation of bacteria by agarose droplets generated by using flow-focusing method. **B.** Generated droplets leave the microfluidic channel through the outlet.

Gelling temperature of the used agarose gel is between 35°C and 38°C. This temperature needs to be kept stable since the polymerization and the crosslinking of the hydrogel is highly correlated with the ambient temperature [14]. Therefore, the experimental setup was kept in an incubation chamber and the ambient temperature was set to 37°C. The gelation process was validated under the microscope and microscopic image taken by the high-speed camera (Hamamatsu Orca-Flash4.0, Japan) is shown in **Fig 4.6B.** It is also confirmed that the size of the generated agarose hydrogel droplets varies between 100 µm – 110 µm. The generated droplets are collected into a 1.5 milliliter (mL) tube. Then the droplets were washed three times with phosphate buffered saline (PBS) solution. For that purpose, the collection tube was centrifuged at 5000 g for 5 min and oil was removed by pipetting and PBS solution was added following every centrifuge.

4.3.3. Acoustic Trapping of Hydrogel Droplets and Cell Culture by Medium Exchange

Once the hydrogel droplets are generated, they were flown through the acoustofluidic platform. Once adequate number of droplets is flown through the acoustic trapping chamber the flow was stopped by closing the microvalve pneumatically. Then the microvalve in the upper inlet was opened and let the culture media flow through the acoustic chamber. Lysongeny-broth (LB) liquid medium was used to provide the essential nutrients for growing the salmonellae. It was prepared by dissolving 25 grams of LB broth powder into a 1 L of purified water. Following that, the solution was autoclaved for 20 minutes at 15 pounds per square inch (psi) on liquid cycle.

In **Fig. 4.7A** trapping of single hydrogel droplet by acoustophoresis can be seen. To keep the droplet in the center the frequency of sinusoidal wave which is applied to PZT is 1.08 MHz and the peak to peak voltage at the ends of the power amplifier is set to be 150 mV. While trapping the droplet the microvalve at the inlet for droplet flow was closed pneumatically and the other microvalve was opened and LB liquid medium was flown through the trapping chamber at a flow rate of 50 µL/h. Since the agarose droplets are porous culture media could diffuse into the droplet and let salmonella grow gradually. After two hours of culture fluorescent microscopic image (**Fig. 4.7B**) was taken to show in-droplet salmonella growth. Colonies became visible after four hours of culture as seen in **Fig. 4.7C**. It is very common to use fluorescence microscopy to observe and analyze the bacterial growth in a culture medium [15].

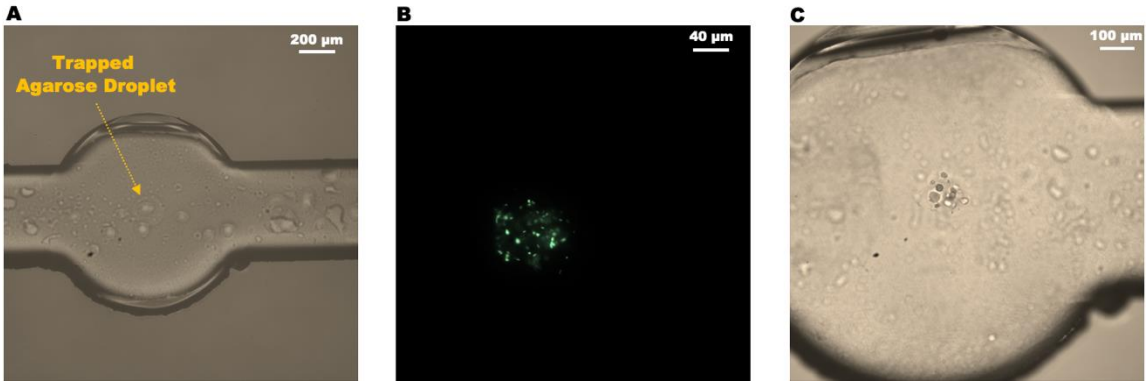

Figure 4.7 A. Brightfield (exposure time: 10 ms) microscopic image to show trapped single agarose droplet. **B.** Green fluorescent (exposure time: 1 s) microscopic image to show salmonella growth after 2 hours – magnified 50x. **C.** Brightfield (exposure time: 10 ms) microscopic image to show salmonella colonies in a single agarose droplet (center of the chamber) after 4 hours.

Similarly, Time-lapse green fluorescent microscopic images of trapped four droplets were taken under the fluorescent upright microscope (Eclipse LV100D, Nikon Inc, Japan) and shown in **Fig. 4.8A-C**. As seen from the microscopic images green fluorescence signal started to be grabbed after two hours. Salmonellae colonies were also checked under the brightfield microscopic illumination and the image was shown in **Fig. 4.8D**. As seen from this image salmonellae can be encapsulated in hydrogel droplets and after trapping those droplets by the help of acoustophoresis medium surrounding the droplets can be changed from PBS to LB medium. Since LB media provide the essential nutrients for bacterial growth salmonella screening was successfully implemented on an acoustofluidic platform.

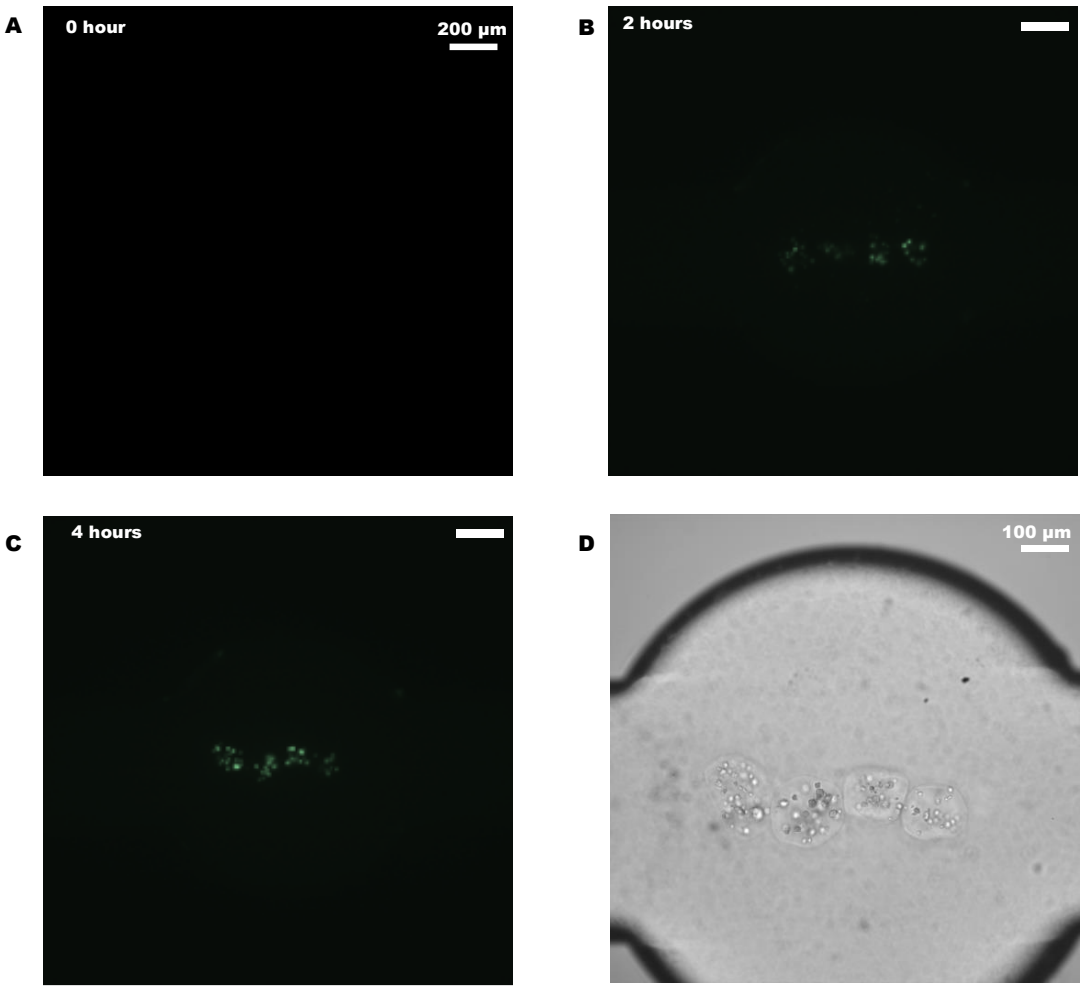

Figure 4.8 A-C. Time-lapse green fluorescent microscopic images (taken at every 2 hours) to show salmonellae growth (exposure time:500 ms and magnified 10 times). **D.** Brighfield microscopic image to show bacterial growth after 4 hours (exposure time:10 ms and magnified 20 times).

Assessment of bacterial growth was determined by green fluorescent protein (GFP) expression of salmonellae. Since the magnification was ten times to capture the whole chamber GFP signal of bacteria inside the droplet could be only be seen after some time of culture. To be able to grab GFP signal of bacterial colonies at least two hours of culture needed to be implemented as shown on **Fig. 4.8B**. This experimental result proves

that researchers/scholars in acoustofluidics can implement on-chip cell screening by taking advantage of acoustophoresis with microvalve actuation. Therefore, cells screening on an acoustofluidic system can be performed for some period of time under the microscope and without needing to change any syringe or tubing, medium surrounding the cells can be exchanged by the help of integrated microvalves. Since this platform was designed to gain the attribute of on-chip flow control of acoustofluidic platforms only four microvalves were fabricated. Because of ease of fabrication number of microvalves can be increased on a single acoustofluidic platform.

4.4. Conclusion

Though acoustofluidic platforms has many benefits such as label-free and high throughput manipulation it lacks some basic attributes of microfluidic chips such as on-chip flow control. In this work, pneumatically actuated microvalves were successfully integrated by the help of PDMS membrane because elasticity and biocompatibility of PDMS let us take advantage of PDMS to use as a microvalve structure. Also in this acoustofluidic platform trapping capability of acoustic microfluidic chips has been attributed so that particle/cell could be trapped in a circular chamber by the help of acoustophoresis. For that reason, hydrogel droplets including cells were successfully trapped at the center of trapping chamber and changing the medium surrounding the hydrogel droplets by the help of microvalve structure let us observe the cell growth inside the hydrogel droplets. This platform could be promising for future studies since it let acoustofluidic platforms acquire the ability to control flow on-chip.

References

1. Wiklund M. Acoustofluidics 12: Biocompatibility and cell viability in microfluidic acoustic resonators. Lab on a Chip. 2012;12(11):2018-28.
2. Antfolk M, Magnusson C, Augustsson P, Lilja H, Laurell T. Acoustofluidic, label-free separation and simultaneous concentration of rare tumor cells from white blood cells. Analytical chemistry. 2015 Sep 3;87(18):9322-8.
3. Lenshof A, Magnusson C, Laurell T. Acoustofluidics 8: Applications of acoustophoresis in continuous flow microsystems. Lab on a Chip. 2012;12(7):1210-23.
4. Lenshof A, Ahmad-Tajudin A, Jarås K, Sward-Nilsson AM, Åberg L, Marko-Varga G, Malm J, Lilja H, Laurell T. Acoustic whole blood plasmapheresis chip for prostate specific antigen microarray diagnostics. Analytical chemistry. 2009 Jul 13;81(15):6030-7.
5. Spengler JF, Jekel M, Christensen KT, Adrian RJ, Hawkes JJ, Coakley WT. Observation of yeast cell movement and aggregation in a small-scale MHz-ultrasonic standing wave field. Bioseparation. 2001;9:329-41.
6. Ding X, Li P, Lin SC, Stratton ZS, Nama N, Guo F, Slotcavage D, Mao X, Shi J, Costanzo F, Huang TJ. Surface acoustic wave microfluidics. Lab on a Chip. 2013;13(18):3626-49.
7. Lenshof A, Evander M, Laurell T, Nilsson J. Acoustofluidics 5: Building microfluidic acoustic resonators. Lab on a Chip. 2012;12(4):684-95.
8. Dual J, Hahn P, Leibacher I, Möller D, Schwarz T, Wang J. Acoustofluidics 19:

Ultrasonic microrobotics in cavities: devices and numerical simulation. Lab on a Chip. 2012;12(20):4010-21.

9. Shin YS, Cho K, Lim SH, Chung S, Park SJ, Chung C, Han DC, Chang JK. PDMS-based micro PCR chip with parylene coating. Journal of Micromechanics and Microengineering. 2003 Jun 20;13(5):768.
10. Park JM, Cho YK, Lee BS, Lee JG, Ko C. Multifunctional microvalves control by optical illumination on nanoheaters and its application in centrifugal microfluidic devices. Lab on a Chip. 2007;7(5):557-64.
11. Abate AR, Agresti JJ, Weitz DA. Microfluidic sorting with high-speed single-layer membrane valves. Applied Physics Letters. 2010 May 17;96(20):203509.
12. Leibacher I, Schatzer S, Dual J. Impedance matched channel walls in acoustofluidic systems. Lab on a Chip. 2014;14(3):463-70.
13. West JL. Bioactive hydrogels: mimicking the ECM with synthetic materials. InScaffolding in tissue engineering 2005 Aug 19 (pp. 275-281). CRC Press.
14. Kumachev A, Greener J, Tumarkin E, Eiser E, Zandstra PW, Kumacheva E. High-throughput generation of hydrogel microbeads with varying elasticity for cell encapsulation. Biomaterials. 2011 Feb 1;32(6):1477-83.
15. Leveau JH, Lindow SE. Predictive and interpretive simulation of green fluorescent protein expression in reporter bacteria. Journal of bacteriology. 2001 Dec 1;183(23):6752-62.

5. INTEGRATION OF DROPLETS INTO ACOUSTOFLUIDICS

5.1. Introduction

In last two decades there has been an increasing development in microfluidic platforms. As being one of the analytical methods in microfluidics field droplet-based microfluidics has shown tremendous progress since the pioneering study conducted by Quake *et. al*. [1]. Droplet microfluidics is a research and technology field to manipulate and deal with small volumes of fluids (μL to pL) through immiscible phases inside microfluidic channels [2]. Being compatible with different biological and chemical reagents and capability of being programmable and configurable made them interesting for scholars in microfluidics [3]. There has been an increasing interest into droplet microfluidics after their blooming. Generation [4,5], splitting [6], merging with each other [7,8], trapping [9], and sorting of droplets [10, 11] are the most common manipulation techniques to name a few. To manipulate droplets some conventional microfluidic methods to sort cells/particles have been combined with droplet-based microfluidics and some of them are dielectrophoresis [12], hydrodynamic [13], optical-based [14], acoustophoresis [15] etc. As mentioned earlier acoustofluidics is a great method to control cells/particles in a microfluidic channel since it makes high-throughput, label-free and contactless manipulation available. Similarly, droplet microfluidics has lots of advantages such as high throughput, scalability, and letting user implement simultaneous experiments. It is obvious that combining these two technologies will provide great benefits in fundamental and applied research. Fornell *et. al.* has shown that enrichment of

microparticles inside droplets can be implemented by acoustophoretic force [16]. In that study a flow focusing droplet generator (**Fig. 5.1**) was designed and acoustic wave was applied to the microfluidic chip so that microparticles could be moved to acoustic pressure nodes. In that study olive oil was used as a spacer between aqueous phase droplets. Since density of olive oil and water is very close this might cause some instability to generate acoustic resonance. In this study we used T-junction droplet generator and a higher density fluid to generate droplets and acoustic positioning is implemented by PZT actuation. Since difference in fluid density let us generate compact and stable droplets. Therefore, acoustic wave disturbance could be minimized while microparticles are trying to be focused at acoustic pressure nodal planes.

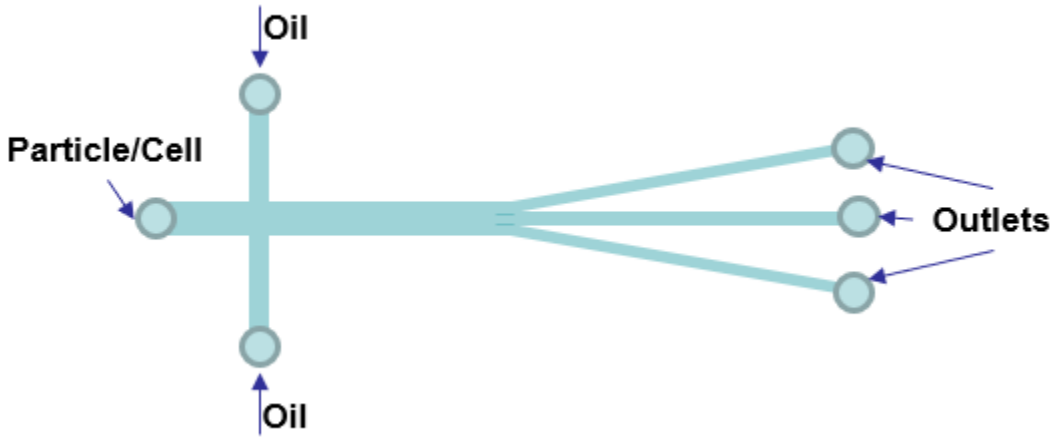

Figure 5.1 Illustration of flow focusing droplet generator with three outlets.

As illustrated in **Fig. 5.2** microparticles encapsulated by the droplets are focused at ¼ and ¾ in λ (full wave) mode, or at middle of the microchannel at λ/2 (half wave) mode.

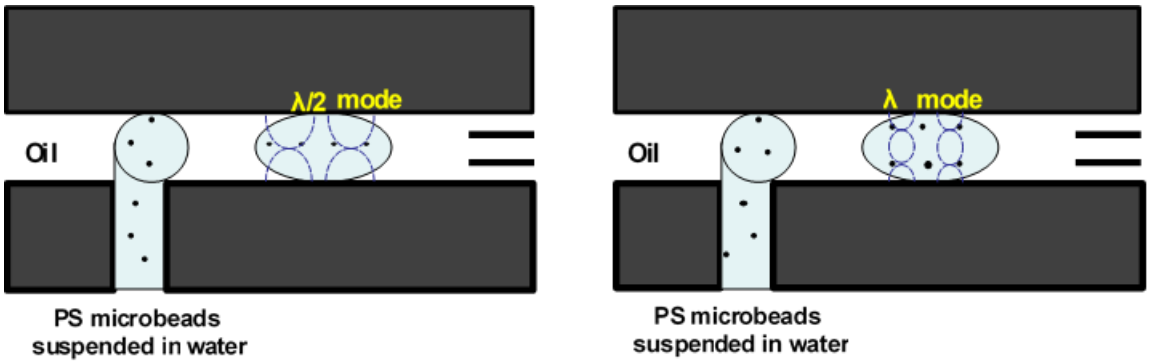

Figure 5.2 Illustration of polystyrene particles under acoustophoretic force, λ (full wave) mode **(A)**, λ/2 (half wave) mode **(B)** when they are encapsulated by the water in oil droplets.

5.2. Materials and Methods

Acoustofluidic device to characterize the trapping capability of different chamber was fabricated by using the following steps. First, the microfluidic channel designs were patterned by photolithography on a silicon wafer and then etched into the silicon substrates using deep reactive ion etching (DRIE) to a depth of 105 µm. Fluidic access holes were drilled in a borosilicate glass substrate using a diamond-plated drill bit mounted on a benchtop drill press (DP101, Ryobi Ltd, SC, USA). The glass and silicon layer were anodically bonded at 420 °C by applying 710 V of DC voltage for one hour. Following the bonding process, ferrules (P200-N, IDEX Health & Science, WA, USA) were glued onto the holes of the glass layer using epoxy for fluidic access. Flexible polymer tubings (Tygon, Saint Gobain Performance Plastics, OH, USA) were inserted inside the ferrules and sealed with epoxy (Gorilla Glue, OH, USA). Following the device packaging channel surface was treated with Repel-ES silane (GE Healthcare, IL, USA) to increase the hydrophobicity. The PZ26 type PZT (Ferroperm, Denmark) was bonded to the bottom of

the chip with cyanoacrylic glue (Loctite, USA), and wires were soldered to the PZT for electrical interconnect.

Acoustofluidic device testing was conducted under an upright microscope (Eclipse LV100D, Nikon Inc, Japan) and fluids were flown through the microchannels by a 4-barrel syringe pump (Fusion 400, Chemyx Inc, MA, USA). Novec 7500 HFE (3M Corp, MN, USA) was used as a spacer between the droplets. The flow rate for microparticles was chosen to be 80 µL/h and the flow rate for spacer was chosen to be 400 µL/h. Fluorescent polystyrene microspheres (Thermoscientific, CA, USA) mixed with de-ionized (DI) water was used for all experiments for easy visualization of particle movement. A function generator (AFG3021B, Tektronix Inc, OR, USA) was utilized to generate a sinusoidal signal that was amplified through a 50-dB power amplifier (2100L, E&I, Ltd.) and applied to the PZT.

In **Fig. 5.3** droplet formation and microparticle encapsulation by the droplet in the silicon microchannel under the upright microscope is shown. As seen from the image channel hydrophobicity is good enough to let compact and stable droplets flow through the microfluidic channel.

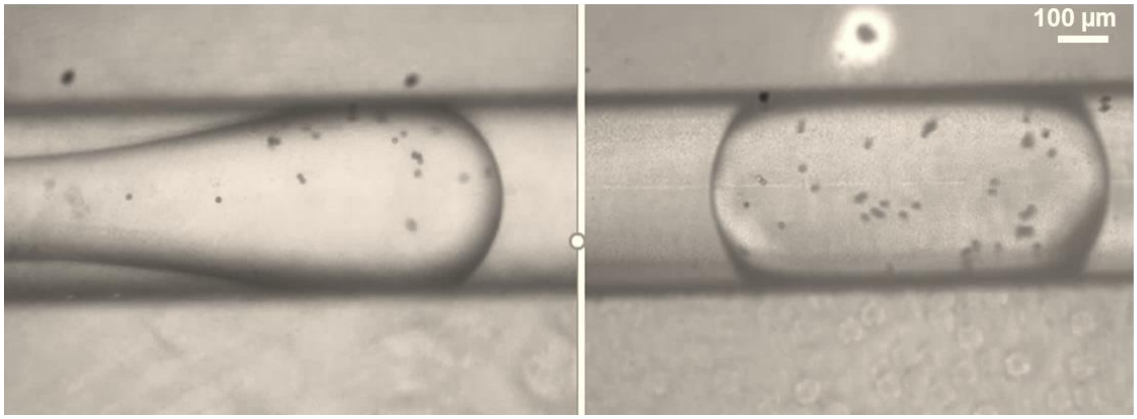

Figure 5.3 Droplet formation **(left)** and encapsulated 12 µm PS microbeads were moving randomly inside the droplet **(right)**.

5.3. Intra-droplet Particle Focusing Using Acoustophoresis

Once the compact and round-shape droplets are generated using the acoustic microfluidic platform PZT at the bottom was actuated at different resonant frequencies so that characterization of the microfluidic chip was successfully implemented. For that purpose, the PZT was run at 2.02 MHz by applying a peak-peak voltage of 150 mV. This actuation successfully migrated the 12 µm polystyrene microspheres to the middle of the silicon microfluidic channel. As shown in **Fig. 5.4** PS microbeads encapsulated by the droplet are successfully focused into the middle of the silicon channel.

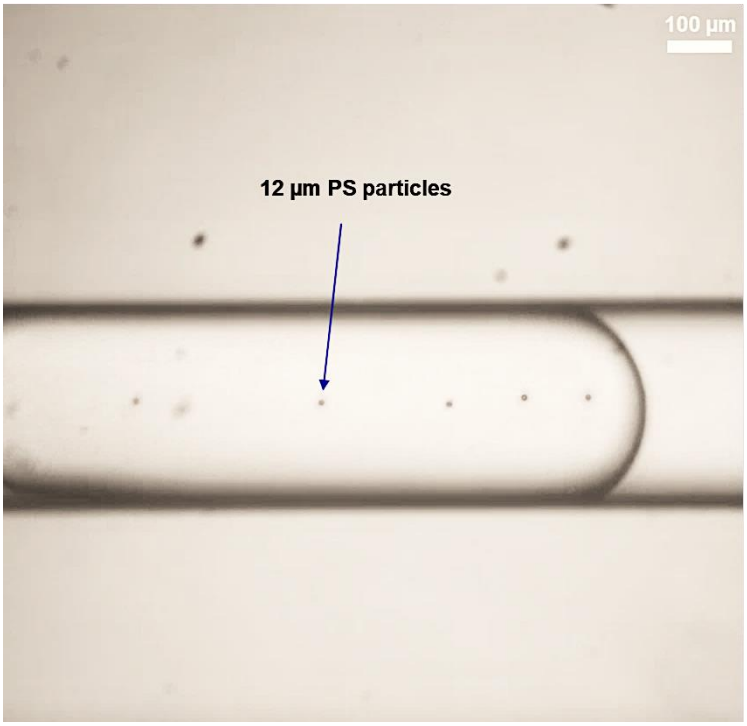

Figure 5.4 Encapsulated 12 µm PS microbeads inside the droplet migrated into middle of the channel at λ/2 (half wave) mode and leaving the acoustofluidic device.

Similarly, when the frequency applied to the PZT was set to 4.04 MHz and the peak-peak voltage before amplified by the RF power amplifier was set to 240 mV PS microbeads inside the droplet were successfully migrated to the $1/4^{th}$ and $3/4^{th}$ of microfluidic channel width and successfully left the chip from the trifurcation of the outlet. Focusing of PS microspheres to acoustic pressure nodes was shown in **Fig. 5.5.**

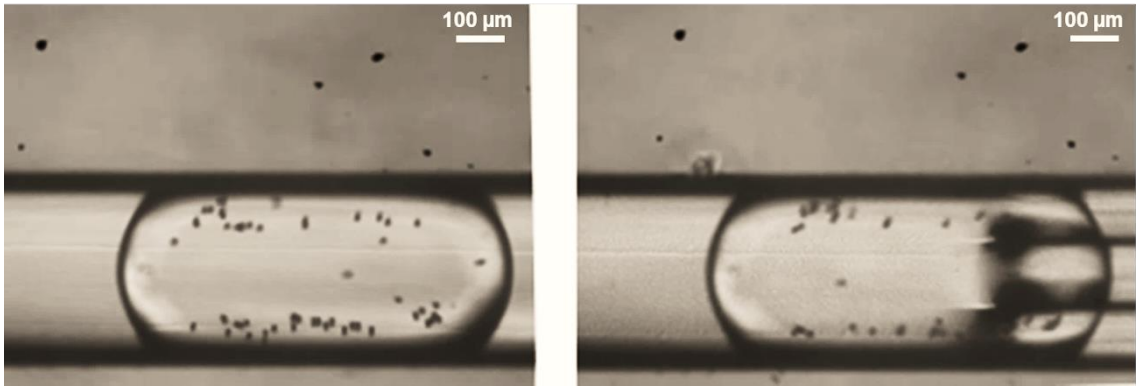

Figure 5.5 Encapsulated 12 µm PS microbeads inside the droplet were moving to acoustic pressure node at λ (full wave) mode (left) and leaving the acoustofluidic device (right).

5.4. Conclusion

Droplet microfluidics is another rapidly growing field in the broad range of microfluidics and because of its throughput, scalability, and letting parallel experimental runs at the same time it is highly appreciated by the scholars in microfluidics. To benefit from this technology acoustofluidic platform which is capable of generating droplets was fabricated. Fabricated acoustofluidic chip was tested for functionality to encapsulate microparticles and manipulate them by the help of acoustophoresis. Successful demonstration of migrating microparticles to the middle and first/third quarters of the microfluidic channel was implemented. This acoustofluidic chip can be developed further to run parallel experiments to manipulate microparticles or droplets using the acoustophoresis.

References

1. Thorsen T, Roberts RW, Arnold FH, Quake SR. Dynamic pattern formation in a vesicle-generating microfluidic device. Physical review letters. 2001 Apr 30;86(18):4163.
2. Shang L, Cheng Y, Zhao Y. Emerging droplet microfluidics. Chemical reviews. 2017 May 24;117(12):7964-8040.
3. Teh SY, Lin R, Hung LH, Lee AP. Droplet microfluidics. Lab on a Chip. 2008;8(2):198-220.
4. Anna SL, Bontoux N, Stone HA. Formation of dispersions using "flow focusing" in microchannels. Applied physics letters. 2003 Jan 20;82(3):364-6.
5. Garstecki P, Fuerstman MJ, Stone HA, Whitesides GM. Formation of droplets and bubbles in a microfluidic T-junction—scaling and mechanism of break-up. Lab on a Chip. 2006;6(3):437-46.
6. Christopher GF, Bergstein J, End NB, Poon M, Nguyen C, Anna SL. Coalescence and splitting of confined droplets at microfluidic junctions. Lab on a Chip. 2009;9(8):1102-9.
7. Cho SK, Moon H, Kim CJ. Creating, transporting, cutting, and merging liquid droplets by electrowetting-based actuation for digital microfluidic circuits. Journal of Microelectromechanical systems. 2003 Feb 28;12(1):70-80.
8. Gu H, Duits MH, Mugele F. Droplets formation and merging in two-phase flow microfluidics. International journal of molecular sciences. 2011 Apr;12(4):2572-97.

9. Huebner A, Bratton D, Whyte G, Yang M, Demello AJ, Abell C, Hollfelder F. Static microdroplet arrays: a microfluidic device for droplet trapping, incubation and release for enzymatic and cell-based assays. Lab on a Chip. 2009;9(5):692-8.
10. Mazutis L, Gilbert J, Ung WL, Weitz DA, Griffiths AD, Heyman JA. Single-cell analysis and sorting using droplet-based microfluidics. Nature protocols. 2013 May;8(5):870.
11. Niu X, Zhang M, Peng S, Wen W, Sheng P. Real-time detection, control, and sorting of microfluidic droplets. Biomicrofluidics. 2007 Dec 3;1(4):044101.
12. Hunt TP, Issadore D, Westervelt RM. Integrated circuit/microfluidic chip to programmably trap and move cells and droplets with dielectrophoresis. Lab on a Chip. 2008;8(1):81-7.
13. Chabert M, Viovy JL. Microfluidic high-throughput encapsulation and hydrodynamic self-sorting of single cells. Proceedings of the National Academy of Sciences. 2008 Mar 4;105(9):3191-6.
14. Huebner A, Srisa-Art M, Holt D, Abell C, Hollfelder F, Demello AJ, Edel JB. Quantitative detection of protein expression in single cells using droplet microfluidics. Chemical communications. 2007(12):1218-20.
15. Leibacher I, Reichert P, Dual J. Microfluidic droplet handling by bulk acoustic wave (BAW) acoustophoresis. Lab on a Chip. 2015;15(13):2896-905.
16. Fornell A, Nilsson J, Jonsson L, Periyannan Rajeswari PK, Joensson HN, Tenje M. Controlled lateral positioning of microparticles inside droplets using acoustophoresis. Analytical chemistry. 2015 Oct 9;87(20):10521-6.

6. CONCLUSION

Microfluidic platforms allow us to reduce the subject of the applications to the scale of micrometers. Because of their scalability, in last two decades those platforms were benefited immensely to analyze the basic elements of matter such as particles, droplets or the basic elements of living organisms such as cells, microorganisms. Albeit too many advantages was revealed by the help of experimental studies since the order of subject was decreased from macroscale to micro/nanoscale it also brought some constraints for the scholars who work in this field. For instance; being label-free and high throughput method made acoustic microfluidic technology preferable but the rapid development in last fifteen years has brought some limitations which come across by the researchers in this field. The above dissertation summarizes the efforts to address some of those limitations in acoustofluidics and development of new type of acoustofluidic platforms to eliminate those restrictions.

6.1. Acoustofluidic Microdevice for Robust Control of Pressure Nodal Positions

Being geometry dependent and having fixed pressure nodal planes are one of the major limitations in acoustofluidics. In second section of this dissertation, this constraint was addressed and to solve it, acoustofluidic microdevice with two adjacent microchannels was designed and successfully fabricated as one of the microchannels having a staircase structure so that position of the particles/cells could be changed throughout the microchannel without necessity of dynamic change of the fluid or resonant

frequency. Being able to migrate particles/cells inside a single microfluidic platform without changing the flowing fluid or resonant frequency has a great potential to promote the abundant usage of acoustofluidics since manipulation of particles/cells can be done more effectively by the help of this technique.

6.2. Acoustic Pressure Nodal Position Adjustment Through PDMS Wall

The developed acoustofluidic chip is based on the concept of decoupling the acoustic boundary from the fluidic boundary. For that purpose, PDMS wall was successfully integrated into the microfluidic channel in a cost-effective way by the help of soft lithography methods. This fabrication method allows us to fabricate a PDMS slab inside an acoustofluidic channel and successfully separate negative acoustic contrast particles from positive acoustic contrast particles by the help of acoustophoresis. Integration of PDMS structure into acoustic microfluidic channel can be exploited by other scholars so that conventional microfluidic techniques such as filtering can be combined with acoustofluidics by taking advantage of label-free, contactless manipulation of cells/particles in acoustofluidic platforms.

6.3. Acoustic with Integrated Microvalves

Since acoustofluidics is relatively modern technology when compared to other microfluidic techniques it lacks on-chip flow control capability. To let it happen, PDMS membrane was fabricated and successfully integrated onto acoustofluidic chip to actuate on-chip microvalve structure. Cells are successfully cultured by using the developed

acoustofluidic chip since on-chip culture medium exchange was implemented by operating the microvalves on this acoustofluidic platform.

6.4. Intra-droplet Particle Manipulation Using Acoustophoresis

Droplet microfluidics is very beneficial for the researchers in this field because of having high throughput, being scalable, letting cell growth inside a droplet. To take advantage of this technology acoustofluidic platform with droplet generator was designed, developed and tested. Tested acoustofluidic chip demonstrated successful focusing of microparticles to the middle and first and third quarters of the droplets inside microfluidic channel. This microfluidic chip can be modified to separate bigger cells such as macrophage from smaller microorganisms such as bacteria and has a potential to be used for high-throughput particle/cell separation.

APPENDIX A

MASK DESIGNS

A.1. Acoustic Microfluidic Device for Precise Control of Pressure Nodal Positions

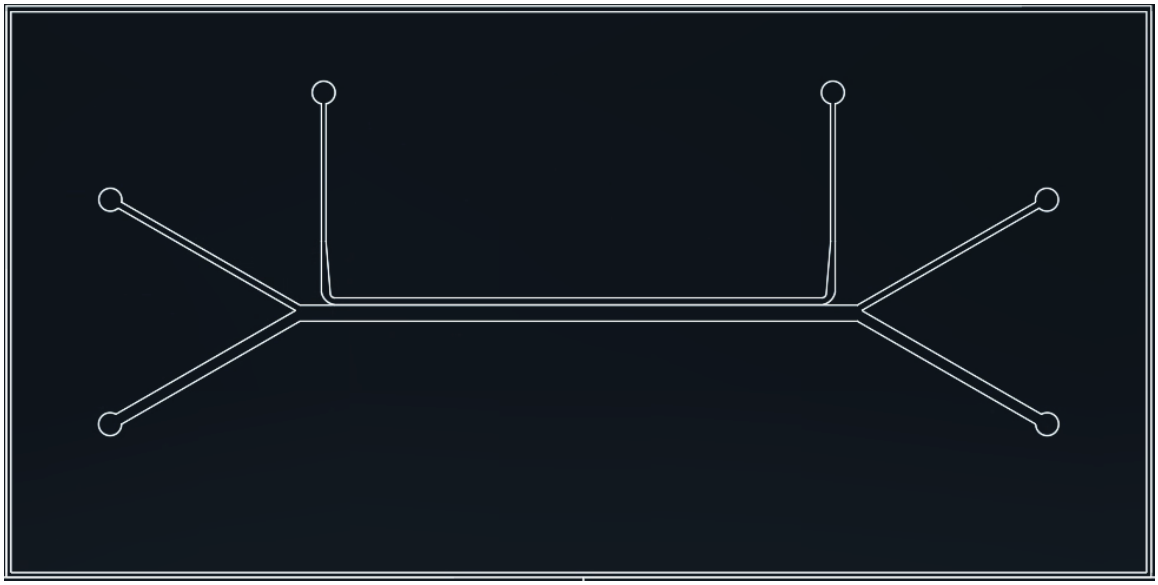

Figure A. 6-1 Mask design for acoustic microfluidic channel with straight echo-channel.

Figure A. 6-2 Mask design for acoustic microfluidic channel with staircase echo-channel.

A.2. Acoustic Microfluidic Device to Decouple the Fluidic Boundary from the Acoustic Boundary

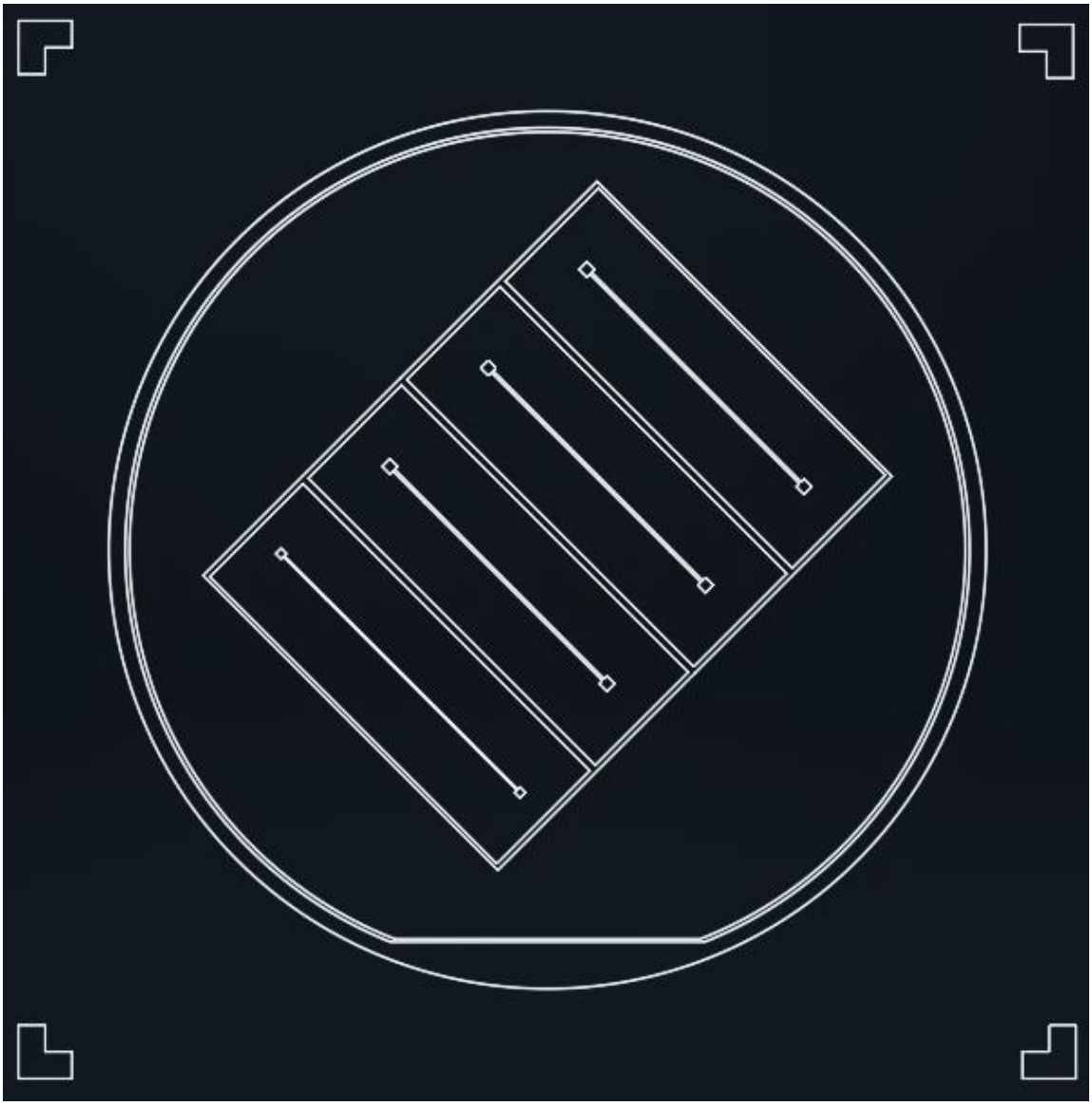

Figure A. 6-3 Mask for acoustic microfluidic device to decouple the fluidic boundary from the acoustic boundary.

A.3. Acoustic Microfluidic Device with Integrated Microvalves

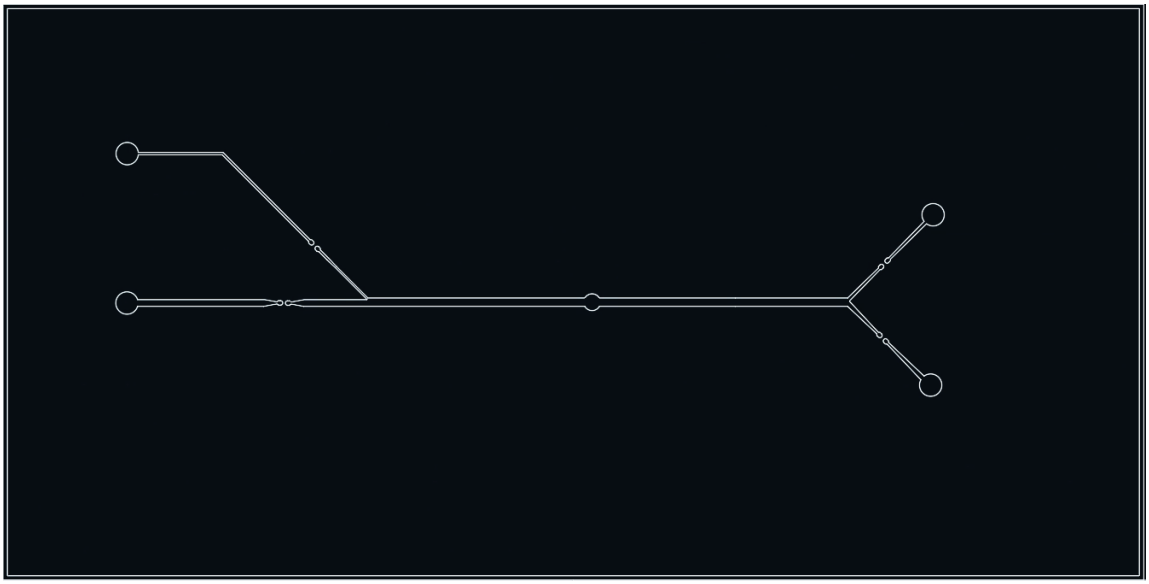

Figure A. 6-4 Mask design for acoustic microfluidic device with integrated microvalves.

A.4. Intra-droplet Acoustofluidic Device

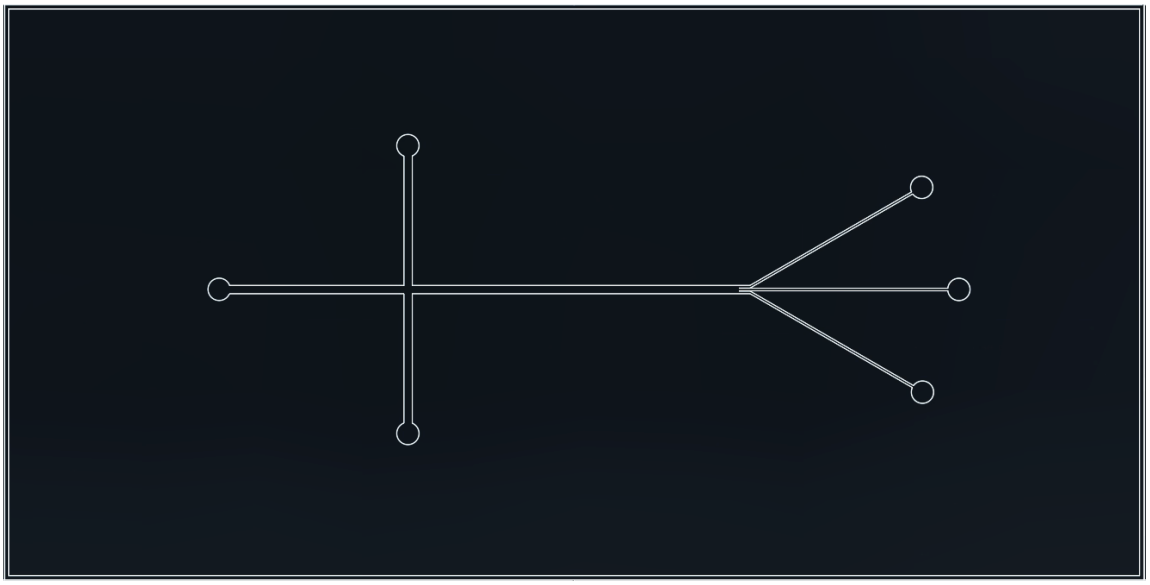

Figure A. 6-5 Mask design for intra-droplet acoustofluidic device

APPENDIX B

SILICON/GLASS ACOUSTOFLUIDIC DEVICE FABRICATION STEPS

B.1. Silicon Etching Procedure

1. Clean the silicon wafers using the piranha cleaning process.
2. Grow a ~1 μm oxide layer on top of the bare silicon wafer using the oxidation furnace.
3. Spin coat AZ5214E positive photoresist (or equivalent) at 3000 rpm for 40 s onto the oxidized wafer.
4. Soft bake the coated wafer at 110°C for 2 min on top of the preheated hotplate
5. Expose that wafer to UV light under Karl Suss MA6 Mask Aligner using the previously designed clearfield pattern mask at 90 mJ/cm^2.
6. Develop the pattern by leaving the wafer in MF726 (or equivalent) for 30 s.
7. Rinse the wafer by DI water.
8. Leave the wafer at 110°C for 2 min.
9. Spin coat the same photoresist at 3000 rpm for 40 s onto the back side of the patterned wafer.
10. Leave the wafer at 110°C for another 2 min.
11. Immerse the patterned wafer into the BOE solution to remove the oxide layer in the exposed area for 15 min.
12. Remove the photoresist using acetone, isopropyl alcohol (IPA) and water.

13. Etch the wafer by immersing it into 40 weight % KOH (s/w) solution at 80°C for the time until the desired depth is achieved.
14. Rinse the wafer by DI water.
15. Remove the oxide layer in the unexposed area by immersing the wafer into BOE solution for another 15 min.
16. Clean the wafer by using DI water and dry it by flowing N_2 gas.

B.2. Glass Etching Procedure

1. Clean the borosilicate glass wafer using the piranha cleaning process.
2. Deposit a uniform Au/Cr layer by using e-beam evaporation equipment (Lesker PVD 75 E-beam Evaporator) of thickness 200/50 nm.
3. Clean the wafer with acetone, IPA and DI water and dry it with N_2 gas.
4. Spin coat AZ5214E positive-photoresist (or equivalent) at 3000 rpm for 40 s onto the oxidized wafer.
5. Soft bake the coated wafer at 110°C for 2 min on top of the preheated hotplate
6. Expose that wafer to UV light under Karl Suss MA6 Mask Aligner using the previously designed clearfield pattern mask at 90 mJ/cm^2
7. Develop the pattern by leaving the wafer in MF726 (or equivalent) for 30 s.
8. Rinse the wafer by DI water.
9. Leave the wafer at 110°C for another 2 min.
10. Immerse the patterned wafer into the Au etchant solution to remove the gold layer in the exposed area for 30 sec.
11. Immerse the patterned wafer into the Cr etchant solution to remove the chromium layer in the exposed area for 30 sec.
12. Remove the photoresist using acetone, isopropyl alcohol (IPA) and water.
13. Cover the back of the wafer with transparent adhesive covers.
14. Etch the wafer by immersing it into 50 v % HF (w/w) solution until the desired depth is achieved.
15. Rinse the wafer by DI water.

16. Remove the Au/Cr layer in the unexposed area by immersing the wafer into Au and Cr etchant solutions, respectively.
17. Clean the wafer by using DI water and dry it by flowing N_2 gas.

B.3. Microfluidic PDMS Layer Fabrication Procedure

1. Coat the master with (tridecafluoro-1,1,2,2-tetrahydrooctyl) trichlorosilane (Gelest, Inc.) by placing the master inside the desiccator chamber with ~4 drops of silane in weigh boat.
2. Coat the master by degassing the chamber for ~30 min.
3. Mix the PDMS base with the curing agent (Sylgard 184 PDMS kist, Dow Corning, Inc.) at 10:1 ratio
4. Pour the PDMS mixture into a weigh boat and degas the mixture using the desiccator for 40 min.
5. Place the coated master in a petri dish and secure it with capton tape.
6. Pour the PDMS mixture on top of the master.
7. Place the petri dish inside the desiccator chamber and degas for 20 min.
8. Cure the PDMS layer in an 85°C until the layer for 4 hours.

B.4. Glass Drilling Procedure

1. Put a mark with a permanent marker for fluidic or pneumatic access hole on top of the borosilicate glass.
2. Attach borosilicate glass to another glass substrate by melting wax between these two substrates.
3. Place a black rubber beneath the bonded substrates as vibration absorber.
4. Add a drop of water on the marks before drilling.
5. Drill the hole using the punch driller with appropriate driller bit.
6. Once the drilling is complete remove wax between two substrates by sonicating them in acetone solution for 30 min.
7. Rinse the substrates by DI water.

B.5. Anodic Bonding

1. Clean the etched silicon substrate and the drilled glass substrate by immersing them into piranha solution for 40 min.
2. Add a drop of water on silicon substrate and align it with glass substrate so that temporary bonding can be implemented.
3. Load them into the bonding equipment by facing the glass substrate down and in contact with ground plate (cathode).
4. Implement the anodic bonding process by applying appropriate force, temperature, and voltage values to the substrates until the bonding is complete.

B.6. Methanol Bonding Procedure

1. Remove the PDMS layer from the master by peeling with tweezer.
2. Punch the fluidic or pneumatic access holes by using a needle of the appropriate size for the tubing.
3. Flow N_2 to remove the dust from the excess PDMS from the hole.
4. Place the glass substrate and the PDMS layer inside the oxygen plasma chamber (Harrick Plasma, Inc., Ithaca, NY).
5. Close the chamber door, valves and vacuum the chamber for 2 min.
6. Apply oxygen plasma treatment to the substrates for 2 min by adjusting the air flow to 10 militorr (mTorr) and setting the chamber to `High` position.
7. Remove the substrates by turning off the vacuum pump and opening the chamber door.
8. Place the substrates on the microscope.
9. Add couple drops of methanol between the substrates and align them under the microscope.
10. Once the methanol is evaporated put the assembled device on 85°C for ~8 hours to complete the bonding process.

APPENDIX C

SALMONELLAE CULTURING AND LYSOGENY BROTH (LB) MEDIUM PREPARATION

C.1. Lysogeny Broth (LB) Media

1. By the help of magnetic stirrer, mix 5 grams of yeast extract, 10 grams of sodium chloride and 10 grams of peptone into a glass bottle filled with a liter of purified water.

2. Sterilize the mixture inside the autoclave for 15 minutes at 120°C and 15 psi.

C.2. Salmonella Culture

1. Add small amount of salmonellae from the agar plate (agar plate is the salmonella banking) to LB medium.

2. Keep the tube with salmonella strains inside the incubator to let them grow overnight at 37°C.

VITA

Name: Sinan Yigit

E-mail Address: sinanyigit06@gmail.com

Education:

Ph.D., Electrical Engineering, Texas A&M University, USA, 2014-2019.

M.S., Electrical Engineering, University of Pittsburgh, USA, 2012-2014.

B.S., Electrical and Electronics Engineering, TOBB University of Economics and Technology, Ankara, Turkey, 2007-2011.

Education Awards:

Fully Funded Study-Abroad Graduate Scholarship from Turkish Ministry of National Education (2012-2019)

Fully Funded Undergraduate Scholarship from TOBB University of Economics and Technology (2006-2011)

Middle School Scholarship from Turkish Ministry of National Education (1999-2003)